

---

# Diagnosing and Mitigating Modality Interference in Multimodal Large Language Models

---

Rui Cai<sup>1</sup> Bangzheng Li<sup>1</sup> Xiaofei Wen<sup>1</sup> Muhao Chen<sup>1</sup> Zhe Zhao<sup>1</sup>

## Abstract

Multimodal Large Language Models demonstrate strong performance on multimodal benchmarks, yet often exhibit poor robustness when exposed to spurious modality interference, such as irrelevant text in vision understanding, or irrelevant visual content in question answering. At its core, modality interference refers to cases where spurious signals from non-essential modalities distort model decisions, which we systematically analyze through causal, perturbation-based diagnostic experiments. To address this problem, we propose a unified finetuning framework that combines heuristic and adversarial perturbation-based data augmentation with output-level consistency regularization between original and perturbed inputs. Extensive experiments across image-heavy, text-heavy, and multimodal benchmarks, spanning multiple MLLM architectures and model scales, demonstrate consistent improvements in unimodal robustness and generalization, while improving standard multimodal performance.

## 1. Introduction

Multimodal Large Language Models (MLLMs) have made significant strides in integrating vision and language understanding within a unified architecture (Liu et al., 2023b; Luo et al., 2023; Bai et al., 2025b). By combining powerful visual encoders and large language models through alignment mechanisms, MLLMs such as LLaVA (Liu et al., 2023b) and Qwen-VL (Bai et al., 2025b) demonstrate strong capabilities across a wide range of multimodal tasks. However, beneath their seemingly impressive performance lies a critical limitation: MLLMs often fail to distinguish between task-relevant and task-irrelevant signals across modalities, leading to unreliable predictions (Wang et al., 2024a; Zhu et al., 2024; Hosseini et al., 2025). A concrete manifestation

of this limitation is their behavior in unimodal diagnostic settings, where only a single modality is required for correct reasoning. In such settings, MLLMs frequently underperform on pure visual recognition (Zhang et al., 2024; Tong et al., 2024) and textual reasoning (Zhu et al., 2024; Wang et al., 2023; Lin et al., 2024), indicating that non-essential modalities can still influence the prediction process.

Recent studies have attributed this failure mode to a variety of learning challenges arising during the multimodal alignment process, such as catastrophic forgetting of pretraining knowledge (Zhang et al., 2024; Tong et al., 2024; Wang et al., 2023; Lin et al., 2024), cross-modality knowledge conflict (Wang et al., 2024a; Zhu et al., 2024), and spurious correlations (Chen et al., 2024a; Hosseini et al., 2025). Catastrophic forgetting has been identified as a key factor in visual degradation (Zhang et al., 2024; Tong et al., 2024), where multimodal tuning of MLLM overrides its pretrained visual features. Cross-modal knowledge conflict (Wang et al., 2024a; Zhu et al., 2024) impairs pure-text reasoning, as models often produce inconsistent outputs when visual inputs are introduced, reflecting misaligned visual and textual parametric memories. Additionally, studies on spurious correlations (Chen et al., 2024a; Hosseini et al., 2025; Zhou et al., 2025) show that MLLMs tend to rely on superficial cross-modal cues rather than task-relevant grounding.

Despite these extensive efforts, existing explanations largely remain fragmented, attributing the observed failures to isolated challenges arising during multimodal alignment. As a result, it remains unclear whether these seemingly diverse issues share a common inference-time mechanism that governs how MLLMs identify and rely on task-relevant modalities during prediction. Motivated by this gap, we adopt a unified perspective and argue that the core limitation lies in MLLMs’ lack of cross-modality competency (Gardner et al., 2021)—the ability to fairly evaluate and integrate information across modalities. Current models lack mechanisms to support this competency during inference, making them vulnerable to misleading cross-modal signals—a failure mode we refer to as *Modality Interference*.

To systematically diagnose and mitigate modality interference, we first design a perturbation-based evaluation experiment inspired by causal intervention principles (Pearl,

<sup>1</sup>Department of Computer Science, University of California-Davis, Davis, CA, United States. Correspondence to: Rui Cai <ruicai@ucdavis.edu>, Zhe Zhao <zao@ucdavis.edu>.

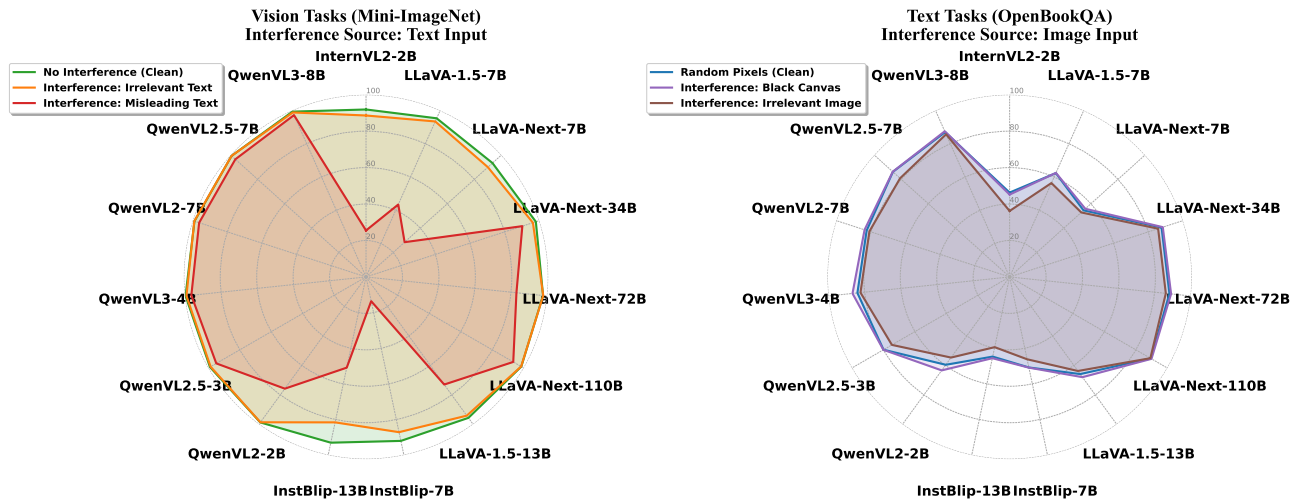


Figure 1. Modality Interference in MLLMs. We visualize the performance of 15 MLLMs using radar charts, where the polygon area signifies model capability. **Left (Vision Tasks):** When vision tasks are interfered with by *Misleading Text* (red), models exhibit a severe performance collapse, shrinking towards the center. **Right (Text Tasks):** Conversely, text reasoning tasks suffer from *Visual Noise* (brown/irrelevant image), causing a noticeable degradation compared to the no-interference baseline.

1995; Chen et al., 2024a), covering multiple tasks and model scales. Specifically, in our analysis, we focus on modality-heavy settings using multiple-choice question answering across image-heavy (e.g., image classification), text-heavy (e.g., pure-text QA), and balanced multimodal tasks (e.g., VQA), enabling controlled analysis under different modality-reliance scenarios. To further induce modality interference, we inject heuristic perturbations (e.g., misleading textual descriptions or distractor visual inputs) into task-irrelevant modalities to introduce spurious or misleading signals, and quantify their impact on model predictions. We evaluate the resulting changes in model predictions to assess the extent of modality interference. While the perturbation-based evaluations offer empirical insights, we further frame our analysis through a causal intervention framework and in which we model this problem through a causal graph abstraction. Building on this framework, we evaluate a range of pretrained MLLMs and observe consistent failure patterns across tasks and scales, as shown in Figure 1. As illustrated, current MLLMs exhibit significant vulnerability to modality interference: misleading textual descriptions trigger a performance collapse in image-heavy tasks, while irrelevant visual noise disrupts text-heavy reasoning.

The empirical results from Figure 1 confirm the presence of modality interference due to their lack of cross-modality competency. To mitigate this, we propose a perturbation-robust fine-tuning framework. We construct a diverse training mixture incorporating both heuristic noise and adversarial worst-case disruptions to simulate alignment failures, while simultaneously employing consistency regularization (e.g., via Jensen–Shannon divergence) to enforce output stability between clean and perturbed inputs. In summary, the main contributions of this paper are threefold. First, we in-

troduce the Cross-Modality Competency Problem to characterize MLLMs’ difficulty in appropriately integrating information across modalities, and identify modality interference as a measurable manifestation of this issue. Second, we propose a causal, perturbation-based evaluation experiment that exposes inappropriate modality reliance and systematically quantifies MLLMs’ susceptibility to task-irrelevant signals. Third, we develop a dataset-agnostic, perturbation-agnostic fine-tuning strategy to mitigate modality interference. Extensive experiments across multiple MLLM families and diverse benchmarks consistently demonstrate the effectiveness and generality of our approach.

## 2. Related Works

**Improving Modality Alignment in Multimodal Language Models** Recent studies have revealed that modality misalignment remains a key obstacle in MLLMs, leading to degraded performance on both image-heavy and text-heavy tasks. For visual understanding, catastrophic forgetting occurs when multimodal tuning overrides pretrained visual features (Zhang et al., 2024; Tong et al., 2024; Wang et al., 2023). In text-heavy scenarios, knowledge conflict (Zhu et al., 2024) arises when inconsistent parametric knowledge from different modalities confuse reasoning. mDPO (Wang et al., 2024a) identifies language bias in training, where models fail to condition their responses on visual input. Some works attribute such issues to shallow fusion (Wang et al., 2023)—e.g., LLaVA (Liu et al., 2023b) uses lightweight projectors to bridge vision and language spaces, leaving a representational gap and resulting in loosely coupled features (Tong et al., 2024; Zhu et al., 2024; Zhao et al., 2025). Others highlight data limitations: even well-encoded visual

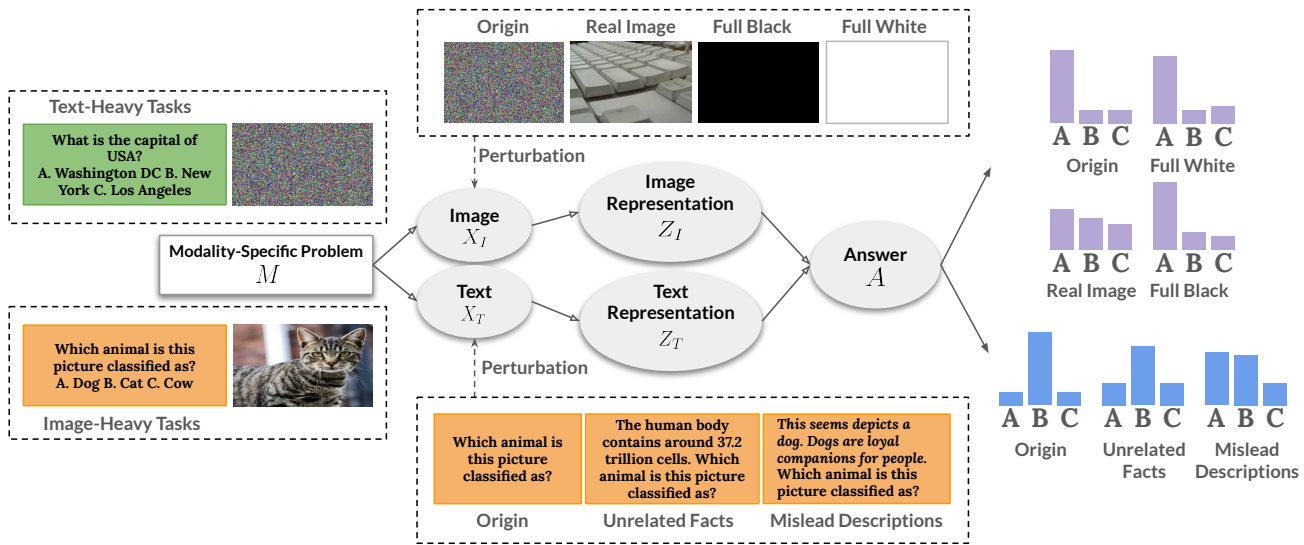


Figure 2. Causal graph illustrating modality interference in our perturbation-based evaluation analysis. Controlled interventions (heuristic) perturb either the image or text inputs, affecting their intermediate representations and ultimately the model prediction.

features fail to support reasoning without adequate supervision to guide decoding (Zhang et al., 2024). Building on these diagnoses, recent works propose multiple solutions. MoF (Tong et al., 2024) mitigates this by fusing features from multiple vision encoders, while VLMClassifier (Zhang et al., 2024) enhances recognition via vision-only finetuning, though it struggles with VQA due to lack of cross-modal alignment. CogVLM (Wang et al., 2023) introduces a visual expert module to improve vision-language integration. VILA (Lin et al., 2024), QwenVL (Bai et al., 2025b), and InternVL (Zhu et al., 2025) incorporate text-only supervision in different ways to preserve or enhance language capabilities during multimodal training—through stage-wise separation, parallel preservation, and unified joint optimization, respectively. Similar patterns also arise in multimodal structural reasoning (Cai et al., 2024). However, these approaches largely treat modality contributions implicitly, without explicitly modeling how multimodal inputs influence the model’s decision process.

**Adversarial Robustness Across Modalities** Adversarial perturbations threaten the reliability of both vision and text models by exploiting vulnerabilities in continuous image embeddings and discrete token spaces. In vision tasks, attacks like FGSM (Goodfellow et al., 2015) and CW (Carlini & Wagner, 2017) first revealed the fragility of neural networks to imperceptible input changes. PGD (Madry et al., 2018) formalized this under a saddle-point framework, becoming the standard for adversarial training. AutoAttack (Croce & Hein, 2020) further unified strong attacks, including PGD variants, into a reliable benchmark. In text tasks, adversarial methods must contend with discrete inputs. TextFooler (Jin et al., 2020) substitutes key words with semantically similar ones to mislead predictions, while CodeAttack (Jha & Reddy, 2023) adapts this idea to code-

language models. More recently, PGD has been extended to LLMs via continuous relaxation (Geisler et al., 2024), enabling efficient attacks in embedding space. PTP (Chen et al., 2023a) applies PGD-style perturbations in the prompt embedding space to smooth training and enhance stability. Inspired by this, our work extends to the multimodal embedding space, enabling unified gradient-based control over both visual and textual inputs with unique masking strategy.

### 3. Causal Analysis on Modality Interference

**Cross-Modality Competency Problems in Multimodal Large Language Models** Competency problems describe scenarios where models rely on spurious correlations between isolated input features and output labels to make predictions, instead of leveraging meaningful interactions among multiple features (Gardner et al., 2021). We extend this concept to the multimodal setting by treating entire modalities (e.g., image  $X_I$  or text  $X_T$ ) as structured feature sources. We define the *Cross-Modality Competency* as an ability for MLLM to fairly evaluate and integrate all modalities, identifying which ones carry task-relevant signals while ignoring misleading or irrelevant ones. In pure-text question answering with MLLMs, the model is provided with both a question and an image, although the image is not required to solve the task. When predictions are influenced by spurious visual cues correlated with certain answers, the model allows irrelevant modality signals to influence its reasoning and predictions, resulting in modality interference.

**Perturbation-based Evaluation Experiment** To systematically measure cross-modality competency, we propose a perturbation-based evaluation framework. The core idea is to inject controlled noise into the irrelevant modality and assess the model’s robustness to such perturbations. Specifi-

cally, for image-heavy tasks, we perturb the text input by: (1) Prepending *unrelated scientific facts*; (2) Prepending *misleading descriptions* that falsely link incorrect options to the image content. For text-heavy tasks, we perturb the visual input by: (1) Attaching a *semantically meaningful real but irrelevant image*; (2) Substituting with a *full black* or *full white* canvas image. Models with strong modality selectivity should maintain high prediction consistency when irrelevant modality signals are perturbed. We select multiple image-heavy and text-heavy tasks for evaluation. Each task is framed as a multiple-choice classification problem, requiring the model to choose the correct option based on image and text modalities as input, with perturbations applied as described above. To validate robustness and generalization for our proposed mitigation method, we additionally consider real-world out-of-distribution perturbations reflecting practical noise encountered in deployed multimodal systems: (i) noisy OCR snippets for image-heavy tasks; and (ii) unrelated UI screenshots for text-heavy tasks. Details in Section 5, Section C.1, Table 8 and Table 11 and Table 12.

**Causal Modeling of Modality Interference** We formalize modality interference through a causal intervention perspective with a causal graph, as shown in Figure 2, where visual inputs ( $X_I$ ) and textual inputs ( $X_T$ ) are processed into their respective representations ( $Z_I, Z_T$ ) before being fused to produce the final prediction ( $A$ ). To study the model’s reliance on different modalities, we introduce perturbations directly at the input level, serving as causal interventions (Pearl, 1995) on  $X_I$  and  $X_T$ . Under ideal cross-modality competency, the model’s prediction should primarily depend on the task-relevant pathway (e.g.,  $X_I \rightarrow Z_I \rightarrow A$  in image-heavy tasks,  $X_T \rightarrow Z_T \rightarrow A$  in text-heavy tasks). Causal interventions at the input level allow us to diagnose whether the model improperly fuses irrelevant signals into its decision process. We use  $x'_I$  to denote an intervention on image  $X_I$  and use  $x'_T$  as an intervention on text  $X_T$ . Following Pearl’s causal framework (Pearl, 1995; int, 2022), we quantify the impact of modality perturbations on model predictions by formalizing causal effects in our multimodal setting. Specifically, we define the pre-intervention prediction distribution as  $P(A|X_I, X_T)$ , and the post-intervention prediction distribution after applying a perturbation on  $X_I$  or  $X_T$  as  $P'(A|\text{do}(X_I = x'_I)$  or  $\text{do}(X_T = x'_T))$ . The *do*-operation represents an intervention to specific modality, and the causal effect (CE) of an intervention is evaluated via a distance metric  $\delta$  comparing  $P$  and  $P'$  as  $\text{CE} = \delta(P, P')$ . We assess the causal effect via prediction changes using  $\delta_{\text{cp}}(P, P') := \mathbb{I}(a \neq a')$  in which  $a = \arg \max_x P(x)$  is the predicted answer before intervention,  $a' = \arg \max_x P'(x)$  is the predicted answer after intervention and  $\mathbb{I}(\cdot)$  is the indicator function that outputs 1 if  $a \neq a'$  and 0 otherwise. Thus,  $\delta_{\text{cp}}$  captures whether the model’s final decision  $A$  changes under perturbations to the input modality. In all interventions, a high value of  $\delta_{\text{cp}}$

indicates the model’s susceptibility to modality interference, revealing spurious reliance on irrelevant modality.

## 4. Methods

To mitigate modality interference and enhance cross-modality competency, we propose a unified perturbation-aware training framework that introduces interventions at both the input level (on  $X_I$  and  $X_T$ ) and the representation level (on  $Z_I$  and  $Z_T$ ) with consistency regularization. Overall pipeline is displayed in Figure 3.

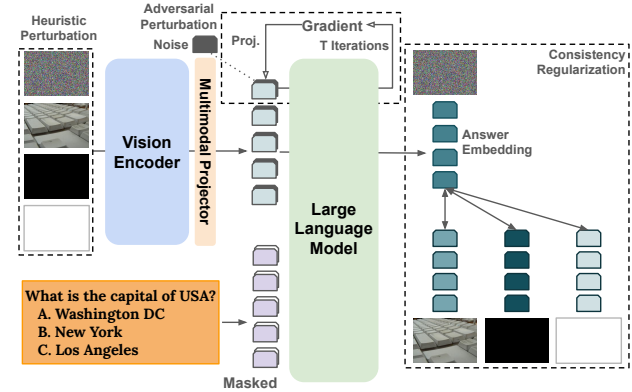


Figure 3. Overview of our proposed framework.

### 4.1. Perturbation-based Data Augmentation

To increase causal robustness along the desired paths  $X_I \rightarrow Z_I \rightarrow A$  (for image-heavy tasks) or  $X_T \rightarrow Z_T \rightarrow A$  (for text-heavy tasks), we first adopt a causally grounded data augmentation method by augmenting each sample with both heuristic perturbations and training time adversarial perturbations.

**Mixture of Multi-Task Training data with Heuristic Perturbations** Let  $\mathcal{D} = (x_I, x_T, a)$  denote the full multimodal training dataset, where  $(x_I, x_T)$  are the image and text inputs and  $a$  is the ground-truth answer. The dataset  $\mathcal{D}$  can be partitioned into three subsets based on tasks: 1) Image-heavy set  $\mathcal{D}^{\text{img}}$ : samples where visual input  $x_I$  is the dominant information source; 2) Text-heavy set  $\mathcal{D}^{\text{text}}$ : samples where textual input  $x_T$  provides the main reasoning signal; 3) VQA set  $\mathcal{D}^{\text{vqa}}$ : samples from vision-language datasets with naturally balanced multimodal dependencies. In practice, we transform these image-heavy and text-heavy datasets into VQA format to construct  $\mathcal{D}^{\text{img}}$  and  $\mathcal{D}^{\text{text}}$ , and derive VQA samples from the supervised finetuning stage of each MLLM as  $\mathcal{D}^{\text{vqa}}$ . For each sample  $(x_I, x_T, a) \in \mathcal{D}^{\text{img}} \cup \mathcal{D}^{\text{text}}$ , we maintain its original version and apply heuristic perturbation to construct Origin Samples and Perturbation-Augmented Samples. Origin samples are used to reinforce the desired causal path (e.g.,  $X_I \rightarrow Z_I \rightarrow A$ ). Perturbation-augmented samples are variants of the same instance with perturbations applied to the ir-

relevant modality, which are denoted as  $(x_I, \tilde{x}_T, a) \in \mathcal{D}_{\text{pert}}^{\text{img}}$  and  $(\tilde{x}_I, x_T, a) \in \mathcal{D}_{\text{pert}}^{\text{text}}$  where  $\tilde{x}_T$  and  $\tilde{x}_I$  are perturbed text and image respectively. Together, the augmented dataset can be written as:

$$\mathcal{D}^{\text{AUG}} = \mathcal{D}^{\text{img}} \cup \mathcal{D}_{\text{pert}}^{\text{img}} \cup \mathcal{D}^{\text{text}} \cup \mathcal{D}_{\text{pert}}^{\text{text}} \cup \mathcal{D}^{\text{VQA}}. \quad (1)$$

We sample  $N_{\text{img}}$  and  $N_{\text{text}}$  examples from  $\mathcal{D}^{\text{img}}$  and  $\mathcal{D}^{\text{text}}$  to construct  $\mathcal{B}_{\text{orig}}^{\text{img}}$  and  $\mathcal{B}_{\text{orig}}^{\text{text}}$  respectively, and the remaining  $N_{\text{vqa}}$  examples are VQA samples from  $\mathcal{D}^{\text{vqa}}$  to construct  $\mathcal{B}^{\text{vqa}}$ . With dynamically generated perturbed variants for each sample, the final training batch is:

$$\mathcal{B} = \mathcal{B}_{\text{orig}}^{\text{img}} \cup \mathcal{B}_{\text{pert}}^{\text{img}} \cup \mathcal{B}_{\text{orig}}^{\text{text}} \cup \mathcal{B}_{\text{pert}}^{\text{text}} \cup \mathcal{B}^{\text{vqa}}, \quad (2)$$

where  $\mathcal{B}_{\text{pert}}^{\text{img}}$  and  $\mathcal{B}_{\text{pert}}^{\text{text}}$  are perturbation-augmented variants generated from  $\mathcal{B}_{\text{orig}}^{\text{img}}$  and  $\mathcal{B}_{\text{orig}}^{\text{text}}$ , respectively. For the full training batch  $\mathcal{B}$ , which includes both original and perturbed samples, we define the supervised loss  $\mathcal{L}_{\text{sft}}$  as the cross-entropy loss computed over all answer tokens in the ground-truth sequences. Let  $\mathcal{L}_{\text{cls}}(x_I, x_T, a)$  denote the standard autoregressive loss for a sample  $(x_I, x_T, a)$ , then:

$$\mathcal{L}_{\text{sft}} = \frac{1}{|\mathcal{B}|} \sum_{(x_I, x_T, a) \in \mathcal{B}} \mathcal{L}_{\text{cls}}(x_I, x_T, a). \quad (3)$$

### Adversarial Perturbation with Cross-Modality Masking

While heuristic perturbations simulate realistic but limited modality noise at the input level, they may not fully capture the worst-case failure modes of MLLMs, especially under complex spurious alignments in the representation space. To overcome this limitation, we introduce a stronger and more generalizable intervention through adversarial training. These perturbations simulate worst-case alignment disruptions during training, serving as targeted interventions on latent nodes  $(Z_I, Z_T)$  to reveal the *Direct Causal Effect* (DCE) of irrelevant modalities on  $A$ . By optimizing the model under such adversarial conditions, we reduce the model’s reliance on spurious cross-modal signals and reinforce task-relevant causal pathways. Inspired by PGD (Madry et al., 2018; Chen et al., 2023b), we design a tailored perturbation strategy for multimodal token embeddings  $(Z_I, Z_T)$ . Unlike standard PGD that applies coarse sign-based updates, our method introduces two critical modifications: (1) *Modality-specific perturbation masking*, which restricts perturbations to task-irrelevant modalities via a binary mask, thereby transforming noise into targeted causal probes rather than indiscriminate corruption. (2) *Raw-gradient updates*, where we remove the sign operator and apply the raw gradient directly, yielding smoother, more diverse, and more realistic perturbations that better simulate modality interference. Formally, we construct perturbations  $\delta = (\delta_I, \delta_T)$  in the latent space that maximize the model’s predictive loss:

$$\delta = \underset{\|\delta\|_{\infty} \leq \epsilon}{\text{argmax}} \mathcal{L}_{\text{cls}}(f(Z_I + \delta_I, Z_T + \delta_T)), \quad (4)$$

where  $\epsilon$  bounds the perturbation strength and  $f$  is the prediction function. We optimize  $\delta$  through  $n$  raw-gradient steps, updating at each step  $t$  as:

$$\delta^{(t+1)} = \Pi_{\|\delta\|_{\infty} \leq \epsilon} \left( \delta^{(t)} + \alpha \cdot \nabla_{\delta} \mathcal{L}_{\text{cls}}(f(Z + \delta^{(t)})) \right), \quad (5)$$

where  $\alpha$  is the step size,  $\Pi$  projects the noise into the  $\ell_{\infty}$  ball, and  $Z = [Z_I; Z_T]$  is the concatenated embedding. In practice, we integrate a modality-specific binary mask  $M \in \{0, 1\}^{L \times d}$ , where  $L$  is the sequence length and  $d$  the hidden dimension, ensuring that perturbations only affect task-irrelevant tokens. Given multimodal embeddings  $\mathbf{E} \in \mathbb{R}^{L \times d}$ , the perturbed embeddings are:

$$\tilde{\mathbf{E}} = \mathbf{E} + \delta \odot M, \quad (6)$$

with  $\odot$  denoting element-wise masking. We initialize  $\delta$  with Gaussian noise  $\mathcal{N}(0, \epsilon^2)$  and update it for  $T$  steps. The final adversarial objective is  $\mathcal{L}_{\text{adv}} = \mathcal{L}_{\text{cls}}(f(\tilde{\mathbf{E}}))$ .

## 4.2. Consistency Regularization under Perturbations

While perturbation-based augmentation exposes the model to diverse interventions, it does not constrain how intermediate representations  $(Z_I, Z_T)$  should respond, and even small changes in the task-irrelevant modality may cause undesirable shifts in fused features. To address this, we introduce a consistency regularization strategy that enforces *output stability* between original and perturbed inputs, serving as an indirect constraint on  $Z_I$  and  $Z_T$  to mitigate modality interference. By minimizing the divergence between the prediction distributions of original and perturbed inputs, the model is encouraged to maintain invariant behavior along the task-relevant causal paths. Formally, given an original input  $x$  and its perturbed counterpart  $\tilde{x}$ , with predictive distributions  $p_{\theta}(A|x)$  and  $p_{\theta}(A|\tilde{x})$ , the consistency loss follows the general form:

$$\mathcal{L}_{\text{consistency}} = \text{Consistency}(p_{\theta}(A|x) \| p_{\theta}(A|\tilde{x})). \quad (7)$$

In practice, we instantiate this by applying distributional divergence (e.g., KL or JS) at the token level. Let  $l^{\text{orig}}, l^{\text{pert}} \in \mathbb{R}^{L_A \times V}$  denote the pre-softmax logits for the original and perturbed samples, where  $L_A$  is the number of answer tokens and  $V$  the vocabulary size. Using KL divergence with temperature  $\tau$  as an example, the loss becomes (equally apply to image-heavy and text-heavy tasks):

$$\mathcal{L}_{\text{consistency}} = \frac{1}{L_A} \sum_{i=1}^{L_A} \sum_{v=1}^V \text{softmax}\left(\frac{l_i^{\text{orig}}}{\tau}\right)_v \cdot \log \frac{\text{softmax}\left(\frac{l_i^{\text{orig}}}{\tau}\right)_v}{\text{softmax}\left(\frac{l_i^{\text{pert}}}{\tau}\right)_v}. \quad (8)$$

## 4.3. Final Training Objective

Our final training objective integrates both perturbation-based data augmentation and consistency regularization into

Table 1. Evaluation on unimodal and VQA datasets. For unimodal datasets, we report accuracy under the original input (Orig) and the worst-performing perturbation (Perturbed). For VQA datasets, we report accuracy on original setting. Best results are highlighted in bold.

Model Settings	Mini-ImageNet		Caltech-101		OpenBookQA		MMLU		ScienceQA	MM-Bench	Seed-Bench
	Orig	Perturbed	Orig	Perturbed	Orig	Perturbed	Orig	Perturbed	Accuracy	Accuracy	Accuracy
LLaVA-1.5-7B	95.3	43.5	97.0	57.4	62.4	56.4	46.3	45.2	64.5	64.3	63.4
+ CoT (Wei et al., 2022)	81.7	28.9	80.9	36.0	38.8	38.9	39.6	38.7	64.7	65.2	64.1
+ VLMClassifier-1 (Zhang et al., 2024)	15.1	0.0	15.6	0.0	61.5	61.5	47.8	47.5	61.1	36.2	35.9
+ VLMClassifier-2 (Zhang et al., 2024)	15.6	0.0	15.1	0.0	61.8	61.2	47.4	47.8	61.8	35.8	36.0
Ours	<b>98.6</b>	<b>98.4</b>	<b>99.3</b>	<b>98.9</b>	<b>81.8</b>	<b>81.0</b>	<b>51.5</b>	<b>51.0</b>	<b>67.8</b>	<b>73.1</b>	<b>64.6</b>
LLaVA-1.5-13B	95.6	73.0	97.9	77.4	65.9	63.8	51.8	50.8	66.1	72.1	64.5
+ CoT (Wei et al., 2022)	92.9	62.8	96.6	67.8	55.6	53.0	47.3	45.5	65.6	70.2	64.9
+ I-MoF (Tong et al., 2024)	93.9	70.1	97.8	80.9	69.2	64.5	46.2	39.1	<b>66.8</b>	73.0	66.6
Ours	<b>98.5</b>	<b>98.4</b>	<b>99.2</b>	<b>98.6</b>	<b>83.0</b>	<b>82.1</b>	<b>56.6</b>	<b>55.8</b>	62.6	<b>73.7</b>	<b>68.4</b>
Qwen2.5-VL-7B	99.3	96.3	99.1	97.2	85.9	77.5	69.3	63.7	85.1	86.6	77.0
+ CoT (Wei et al., 2022)	99.1	91.4	98.5	92.5	77.8	68.8	61.5	57.4	85.2	86.7	77.1
R1-OneVision-7B (Yang et al., 2025)	98.2	87.7	96.5	84.7	81.2	77.6	63.2	60.8	84.5	85.4	76.3
Ours	<b>99.6</b>	<b>99.5</b>	<b>99.6</b>	<b>99.7</b>	<b>90.9</b>	<b>89.7</b>	<b>69.8</b>	<b>68.2</b>	83.9	<b>87.0</b>	<b>78.3</b>

a unified framework. For each batch, we begin with a set of original samples  $\mathcal{B}_{\text{orig}}$  and dynamically construct their heuristic perturbed counterparts  $\mathcal{B}_{\text{pert}}$  via input-level augmentations. We then apply adversarial perturbations on both  $\mathcal{B}_{\text{orig}}$  and  $\mathcal{B}_{\text{pert}}$ , and enforce consistency between the original and all perturbed samples. The overall loss is:

$$\mathcal{L}_{\text{total}} = \mathcal{L}_{\text{sft}} + \mathcal{L}_{\text{adv}} + \lambda_{\text{cons}} \cdot \mathcal{L}_{\text{consistency}}, \quad (9)$$

where  $\mathcal{L}_{\text{sft}}$  is the supervised loss computed over  $\mathcal{B}$ ,  $\mathcal{L}_{\text{adv}}$  is the adversarial loss computed on all adversarial perturbed samples and  $\mathcal{L}_{\text{consistency}}$  is the consistency loss between original and all perturbed sample pairs. By aligning all three losses with the causal structure of multimodal reasoning, we systematically mitigate modality interference and improve cross-modality competency in MLLMs.

## 5. Experiments

**Models.** We conduct experiments on three MLLM families with different parameter size: Qwen2.5-vl-3b (Bai et al., 2025b), LLaVA-1.5-7B & LLaVA-1.5-13B (Liu et al., 2023a) and InstructBLIP-Vicuna-7B (Luo et al., 2023). Following LLaVA and Qwen-VL, we freeze the vision encoder and train the multimodal projector and language model; for InstructBLIP, we instead freeze both the vision encoder and Q-Former, fine-tuning only the projection layer and language model (see Section B).

**Baselines.** We include following baselines for comparison: *LLaVA-1.5-13B + I-MoF* (Tong et al., 2024): By applying the designed Interleaved Mixture-of-Features (I-MoF) module on LLaVA-1.5-13B to spatially combine CLIP (Radford et al., 2021) and DINOv2 (Oquab et al., 2023) visual tokens, it enhances visual grounding by integrating complementary features from contrastive and self-supervised vision encoders. *VLMClassifier* (Zhang et al., 2024): it enhances visually-grounded language models for image classification by fine-tuning them on ImageNet (Deng et al., 2009) (*VLMClassifier-1*) or ImageNet combining LLaVA-Instruct (Liu et al., 2023b) (*VLMClassifier-2*). *R1-OneVision-7B* (Yang et al., 2025): a reasoning-enhanced

“thinking” model built upon the Qwen2.5-VL-7B backbone. We include it to investigate whether intrinsic reasoning capabilities can inherently mitigate modality interference. *Chain-of-Thought (CoT) Prompting* (Wei et al., 2022): we further evaluate prompt-based mitigation by encouraging structured reasoning through CoT-style prompting. The specific prompt design and results are reported in Section C.4. **Datasets.** We evaluate models on benchmarks covering three task types: (i) *Image-heavy tasks*: Mini-ImageNet (Russakovsky et al., 2015) and Caltech-101 (Fei-Fei et al., 2004), used in both training and evaluation; (ii) *Text-heavy tasks*: OpenBookQA (Mihaylov et al., 2018) and MMLU (Hendrycks et al., 2020), used in both training and evaluation; (iii) *VQA tasks*: For training, we use LLaVA-Instruct-dataset (Liu et al., 2023b) as the instruction-tuning dataset for related models. For InstructBLIP, we additionally use TextCaps (Sidorov et al., 2020) following its original training configuration. For Qwen2.5-VL, whose instruction-tuning data is proprietary, we adopt LLaVA-Instruct as a standardized alternative. For evaluation, we adopt three multiple-choice VQA benchmarks: ScienceQA-IMG (Lu et al., 2022), MM-Bench-EN (Liu et al., 2023c), and Seed-Bench-IMG (Li et al., 2023). For ScienceQA and Seed-Bench, we only include examples with image context. For MM-Bench, we use the English version. All datasets are converted into a unified multiple-choice VQA format. We report the accuracy of model predictions and quantify the causal effect with the prediction change rate  $\delta_{\text{cp}}$ . All models are fine-tuned for 1 epoch with a fixed batch size  $N_{\text{batch}}$ . All the hyperparameters are listed in Section D. For each dataset, results are averaged over multiple independent runs. Following standard practice, inference is performed with deterministic decoding (temperature fixed at 0).

**Achieving Pareto-Optimality Across Unimodal and Multimodal Tasks** As shown in Table 1, our method outperforms all baselines across different base MLLMs, demonstrating stronger robustness to modality interference. While CoT slightly improves performance in certain VQA settings, its overall gains are minimal and inconsistent, and it fails to mitigate modality interference (e.g., 85.9% vs.

**Diagnosing and Mitigating Modality Interference in Multimodal Large Language Models**

Table 2. Multimodal reasoning accuracy (%) on VQA benchmarks under various ablation study configurations. The best accuracy is marked in bold. Arrows ( $\uparrow/\downarrow$ ) indicate relative changes compared to the Vanilla baseline of each model. Overall performance is computed as a weighted average across datasets, with weights proportional to each dataset’s test size Table 16. (full results in Table 7)

Model	Method	ScienceQA-IMG	MM-Bench-EN	Seed-Bench-IMG	VQA Overall
<b>3B Multimodal Models</b>					
<b>Qwen2.5-VL-3B</b> <small>(Bai et al., 2025b)</small>	Vanilla	63.0 (100%)	81.8 (100%)	72.3 (100%)	72.5 (100%)
	FFT with $D^{VQA}$	72.2 ( $\uparrow$ 14.6%)	82.0 ( $\uparrow$ 0.2%)	74.7 ( $\uparrow$ 3.3%)	75.5 ( $\uparrow$ 3.9%)
	FFT with $D^{AUG}$	73.6 ( $\uparrow$ 16.8%)	81.7 ( $\downarrow$ 0.1%)	75.3 ( $\uparrow$ 4.1%)	<b>76.2 (<math>\uparrow</math>5.1%)</b>
	+ KL	72.8 ( $\uparrow$ 15.6%)	80.9 ( $\downarrow$ 1.1%)	74.9 ( $\uparrow$ 3.6%)	75.9 ( $\uparrow$ 4.7%)
	+ ADV	73.1 ( $\uparrow$ 16.0%)	81.7 ( $\downarrow$ 0.1%)	75.3 ( $\uparrow$ 4.1%)	76.1 ( $\uparrow$ 5.0%)
	Ours	73.8 ( $\uparrow$ 17.1%)	82.1 ( $\uparrow$ 0.1%)	75.5 ( $\uparrow$ 4.4%)	<b>76.4 (<math>\uparrow</math>5.4%)</b>
<b>7B Multimodal Models</b>					
<b>LLaVA-1.5-7B</b> <small>(Liu et al., 2023a)</small>	Vanilla	64.5 (100%)	64.3 (100%)	63.4 (100%)	63.8 (100%)
	FFT with $D^{VQA}$	61.6 ( $\downarrow$ 4.5%)	71.4 ( $\uparrow$ 11.0%)	62.4 ( $\downarrow$ 1.6%)	64.0 ( $\uparrow$ 0.3%)
	FFT with $D^{AUG}$	65.4 ( $\uparrow$ 1.4%)	71.1 ( $\uparrow$ 10.6%)	63.9 ( $\uparrow$ 0.8%)	65.6 ( $\uparrow$ 2.8%)
	+ JS	63.8 ( $\downarrow$ 1.1%)	73.5 ( $\uparrow$ 14.3%)	63.7 ( $\uparrow$ 0.5%)	65.6 ( $\uparrow$ 2.8%)
	+ ADV	66.7 ( $\uparrow$ 3.4%)	71.4 ( $\uparrow$ 11.0%)	63.6 ( $\uparrow$ 0.3%)	65.7 ( $\uparrow$ 3.0%)
	Ours	67.8 ( $\uparrow$ 5.1%)	73.1 ( $\uparrow$ 13.7%)	64.6 ( $\uparrow$ 1.9%)	<b>66.8 (<math>\uparrow</math>4.7%)</b>
<b>13B Multimodal Models</b>					
<b>InstructBLIP-13B</b> <small>(Luo et al., 2023)</small>	Vanilla	65.8 (100%)	72.1 (100%)	63.8 (100%)	65.8 (100%)
	FFT with $D^{VQA}$	61.7 ( $\downarrow$ 6.2%)	68.5 ( $\downarrow$ 5.0%)	56.0 ( $\downarrow$ 12.2%)	59.4 ( $\downarrow$ 9.7%)
	FFT with $D^{AUG}$	66.6 ( $\uparrow$ 1.2%)	71.5 ( $\downarrow$ 0.8%)	64.0 ( $\uparrow$ 0.3%)	65.9 ( $\uparrow$ 0.2%)
	+ KL	67.2 ( $\uparrow$ 2.2%)	72.6 ( $\uparrow$ 0.7%)	64.0 ( $\uparrow$ 0.3%)	66.2 ( $\uparrow$ 0.6%)
	+ ADV	66.1 ( $\uparrow$ 0.5%)	74.0 ( $\uparrow$ 2.6%)	64.1 ( $\uparrow$ 0.5%)	66.4 ( $\uparrow$ 0.9%)
	Ours	66.2 ( $\uparrow$ 0.6%)	73.2 ( $\uparrow$ 1.5%)	64.3 ( $\uparrow$ 0.7%)	<b>66.5 (<math>\uparrow</math>1.1%)</b>

97.9% on Mini-ImageNet). Similarly, even the reasoning-enhanced R1-OneVision-7B suffers from significant degradation (e.g., dropping from 96.5% to 84.7% on Caltech-101), indicating that intrinsic “thinking” capabilities alone are insufficient to resolve the issue. While I-MoF enhances visual grounding by integrating multiple visual features, it still suffers from modality interference: e.g. LLaVA-1.5-13B + I-MoF drops from 93.9% to 70.1% under perturbation ( $\downarrow$ 23.8%), indicating reliance on spurious textual cues. In contrast, our method maintains perturbed performance at 98.4% ( $\downarrow$ 0.1%). On the other hand, VLM-Classifier, adopts vision-only fine-tuning, which leads to critical limitations—vulnerability to cross-modal interference and degradation on VQA tasks, as LLaVA-1.5-7b + VLMClassifier-1 only reaches 35.8%/36.2% on MM-Bench/SeedBench, notably lower than both base LLaVA and our method (73.7%/68.4%), highlighting that vision-centric strategies, without addressing modality alignment, are insufficient for robust multimodal understanding. In text-heavy tasks, our method also achieves superior perturbed performance, indicating that addressing modality interference directly, rather than merely improving representations, is key to robust multimodal reasoning. Overall, unlike prior methods that often trade off between unimodal and multimodal performance, our method consistently improves both, achieving *Pareto-optimality*.

**Ablation Studies** To evaluate the effectiveness of each component in our framework, we conduct a comprehensive

Table 3. Evaluation of Caltech-101 (image-heavy) and MMLU (text-heavy) across different ablation study settings across different model families (full results in Table 6).

Model	Method	Caltech-101		MMLU	
		Orig	Perturbed	Orig	Perturbed
LLaVA-1.5-7B	Vanilla	97.0	57.4	62.4	56.4
	+ $D^{VQA}$	96.2	46.3	61.3	55.5
	+ $D^{AUG}$	98.5	98.6	78.6	77.2
	+KL	98.6	98.7	81.4	81.2
	+ADV	98.7	98.5	81.7	80.8
	Ours	<b>99.3</b>	<b>99.0</b>	<b>81.8</b>	<b>81.5</b>
InstructBLIP-7B	Vanilla	90.3	17.5	50.9	46.2
	+ $D^{VQA}$	92.1	23.1	49.8	45.2
	+ $D^{AUG}$	99.0	56.1	75.0	74.8
	+JS	98.9	<b>98.4</b>	78.0	76.6
	+ADV	99.1	85.2	76.8	76.3
	Ours	<b>99.2</b>	98.3	<b>79.0</b>	<b>78.3</b>

ablation study across multiple models and scales. We compare the pretrained models with the following strategies: *FFT with  $D^{VQA}$*  (standard finetuning on VQA data), *FFT with  $D^{AUG}$*  (supervised finetuning on mixed multi-task datasets with heuristic perturbations), *FFT+KL/JS* (adding consistency regularization on KL or JS divergence), *FFT+ADV* (FFT with heuristic & adversarial perturbations), and *Ours* (combining both perturbation-based data augmentation and consistency regularization). Table 2 presents overall VQA performance, and Table 3 evaluates model robustness under unimodal settings. (Table 5 reports results with all perturbations.) Together, these results show the effectiveness of our method in improving both gen-

Table 4. Evaluation of out-of-distribution (OOD) robustness under *unseen perturbation types* across both image-heavy and text-heavy tasks on all evaluated datasets (Seen: Mini-ImageNet, Caltech-101, OpenBookQA, MMLU; Unseen: Food-101, ARC Challenge).

Model	Method	Image-heavy						Text-heavy					
		Mini-ImageNet		Caltech-101		Food-101		OpenBookQA		MMLU		ARC Challenge	
		Orig	OCR	Orig	OCR	Orig	OCR	Orig	Screenshot	Orig	Screenshot	Orig	Screenshot
LLaVA-1.5-7B	Vanilla	95.3	88.9	97.0	92.8	90.2	83.6	62.4	50.2	46.3	44.8	53.4	51.8
	+D <sup>AUG</sup>	98.2	98.0	98.5	98.0	91.3	83.5	78.6	78.0	51.1	50.6	55.7	53.8
	+ADV	98.7	98.2	98.7	98.4	91.8	86.7	81.7	81.3	50.6	51.3	57.9	57.4
	Ours	<b>98.6</b>	<b>98.2</b>	<b>99.3</b>	<b>99.0</b>	<b>92.1</b>	<b>89.5</b>	<b>81.8</b>	<b>81.2</b>	<b>51.5</b>	<b>51.3</b>	<b>62.8</b>	<b>62.6</b>
InstructBLIP-7B	Vanilla	92.0	81.4	90.3	83.6	67.9	48.0	50.9	40.0	35.3	34.9	33.7	36.5
	+D <sup>AUG</sup>	98.5	95.7	99.0	98.4	55.5	56.5	75.0	74.4	50.0	49.2	27.3	30.7
	+ADV	98.7	97.5	99.5	98.8	93.2	85.9	76.8	76.2	49.3	49.3	50.1	44.5
	Ours	<b>98.4</b>	<b>97.3</b>	<b>99.2</b>	<b>99.0</b>	<b>95.6</b>	<b>88.1</b>	<b>79.0</b>	<b>77.8</b>	<b>50.2</b>	<b>49.2</b>	<b>57.6</b>	<b>57.0</b>
Qwen2.5-VL-7B	Vanilla	99.3	99.2	99.1	99.2	97.1	96.7	85.9	69.3	69.3	57.0	<b>85.6</b>	79.6
	+D <sup>AUG</sup>	99.6	99.5	<b>99.7</b>	99.3	97.1	96.5	90.2	85.8	70.4	63.7	82.9	80.2
	+ADV	99.4	99.5	99.6	<b>99.6</b>	97.3	96.9	91.7	<b>91.5</b>	<b>70.4</b>	69.7	85.0	81.2
	Ours	<b>99.6</b>	<b>99.5</b>	99.6	99.5	<b>97.5</b>	<b>97.4</b>	<b>90.9</b>	90.7	69.8	<b>69.7</b>	84.1	<b>82.6</b>

eral VQA accuracy and robustness under modality interference. Across all model families (Qwen2.5-VL, InstructBLIP, LLaVA-1.5) and model sizes (3B/7B/13B), our method consistently achieves best overall performance, improving accuracy on both unimodal and multimodal benchmarks. For instance, it boosts overall VQA accuracy (e.g., +14.9% on InstructBLIP-7B), but also enhances robustness to modality interference—improve the performance under perturbations by over 50% on image-heavy tasks (e.g. 17.5% → 98.3% with InstructBLIP-7B on Caltech101). We also extend evaluation from MCQA to free-form QA and additional diagnostic experiments, including a no-mask ablation, which exhibit consistent robustness trends (see Sections C.5 and C.7).

We observe consistent improvements across both unimodal and multimodal tasks when moving from  $FFT w/ D^{VQA}$  to  $FFT w/ D^{AUG}$ , highlighting the importance of incorporating modality-specific supervision and heuristic perturbations. Building upon this, adding consistency regularization yields further gains by stabilizing model predictions under controlled perturbations on  $X_I$  or  $X_T$ . Both KL and JS objectives lead to similar improvements, suggesting that the model equally benefits from all heuristic perturbations regardless of anchor choice. To further validate generalization, we introduce two real-world out-of-distribution perturbations at test time: (i) noisy OCR snippets sampled from FUNSD (Jaume et al., 2019) as irrelevant text into image-heavy tasks; and (ii) unrelated UI screenshots from RICO (Deka et al., 2017) as distractor images in text-heavy tasks. Beyond existing datasets, we further evaluate on Food-101 (Bossard et al., 2014) (unseen image-heavy dataset) and ARC-Challenge (Clark et al., 2018) (unseen text-heavy dataset), neither of which is used during training. As shown in Table 4, our method significantly improves robustness under these unseen perturbations with consistent gains (e.g., on InstructBLIP-7B, 83.6% → 99.0% under OCR noise on Caltech-101). Crucially, results on new datasets confirm our method’s strong OOD generalization. Under misleading

text (seen perturbation) and OCR-style noise (unseen perturbation), vanilla models suffer severe degradation, while our method preserves accuracy close to clean-baseline performance. In contrast, heuristic data augmentation alone fails to generalize to unseen noise, and may even degrade performance (e.g., on InstructBLIP-7B, heuristic augmentation degrades performance on Food-101 under clean inputs (67.9% vs. 55.5%). These results demonstrate that **the modest overhead of adversarial training** (see Section E) **yields substantial gains in out-of-domain generalization** (full results in Table 11 and Table 12).

### 6. Conclusion

In this paper, we identify and formalize modality interference as a concrete manifestation of the broader cross-modality competency problem in Multimodal Large Language Models—namely, the inability to distinguish task-relevant from irrelevant modality signals. Through a designed perturbation-based causal evaluation experiment, we demonstrate that even state-of-the-art MLLMs systematically exhibit degraded performance under irrelevant but misleading inputs, revealing a fundamental vulnerability in their inference-time reasoning. To mitigate this issue, we propose a robust fine-tuning strategy that combines modality-specific data augmentation, consistency regularization, and adversarial perturbation in the embedding space. These designs explicitly constrain the model to produce stable outputs under spurious modality shifts, thereby reducing reliance on non-causal correlations and improving robustness. Extensive experiments across diverse architectures, scales, and task regimes confirm that our approach consistently improves both unimodal reasoning and multimodal generalization, achieving Pareto-optimal performance.

## 7. Impact Statement

This paper presents work whose goal is to advance the field of machine learning by improving the understanding and robustness of multimodal large language models. The proposed analyses and training methods aim to make model behavior more reliable under modality-specific perturbations.

The societal impacts of this work are consistent with those commonly associated with advances in machine learning research, and we do not anticipate any unique ethical concerns that require special discussion.

## References

- Probabilistic and causal inference: The works of Judea Pearl. *Probabilistic and Causal Inference*, 2022. URL <https://api.semanticscholar.org/CorpusID:267813400>.
- Bai, S., Cai, Y., Chen, R., Chen, K., Chen, X.-H., Cheng, Z., Deng, L., Ding, W., Fang, R., Gao, C., Ge, C., Ge, W., Guo, Z., Huang, Q., Huang, Q., Huang, F., Hui, B., Jiang, S., Li, Z., Li, M., Li, M., Li, K., Lin, Z., Lin, J., Liu, X., Liu, J., Liu, C., Liu, Y., Liu, D., Liu, S., Lu, D., Luo, R., Lv, C., Men, R., Meng, L. Y., Ren, X., Yi Ren, X., Song, S., Sun, Y.-C., Tang, J., Tu, J., Wan, J., Wang, P., Wang, P., Wang, Q., Wang, Y., Xie, T., Xu, Y., Xu, H., Xu, J., Yang, Z., Yang, M., Yang, J., Yang, A., Yu, B., Zhang, F., Zhang, H., Zhang, X., Zheng, B., Zhong, H., Zhou, J., Zhou, F., Zhou, J., Zhu, Y., and Zhu, K. Qwen3-v1 technical report. *ArXiv*, abs/2511.21631, 2025a. URL <https://api.semanticscholar.org/CorpusID:283262018>.
- Bai, S., Yang, C., Hu, L., Li, X., Wang, Y., Bai, Y., Zhou, X., Guo, S., Deng, G., Cao, T., Lu, Y., Ma, S., Wu, Z., Liu, Z., Fan, Y., Shi, W., Zhou, H., Yin, J., Lin, Z., and Tang, J. Qwen2.5-vl technical report. *arXiv preprint arXiv:2502.13923*, 2025b.
- Bossard, L., Guillaumin, M., and Van Gool, L. Food-101—mining discriminative components with random forests. In *European conference on computer vision*, pp. 446–461. Springer, 2014.
- Cai, R., Pei, S., and Zhang, X. Zero-shot relational learning for multimodal knowledge graphs. In *2024 IEEE International Conference on Big Data (BigData)*, pp. 499–508. IEEE, 2024.
- Carlini, N. and Wagner, D. A. Towards evaluating the robustness of neural networks. In *2017 IEEE Symposium on Security and Privacy, SP 2017, San Jose, CA, USA, May 22-26, 2017*, pp. 39–57. IEEE Computer Society, 2017. doi: 10.1109/SP.2017.49. URL <https://doi.org/10.1109/SP.2017.49>.
- Chen, L., Chen, J., Huang, H., and Cheng, M. PTP: boosting stability and performance of prompt tuning with perturbation-based regularizer. In Bouamor, H., Pino, J., and Bali, K. (eds.), *Proceedings of the 2023 Conference on Empirical Methods in Natural Language Processing, EMNLP 2023, Singapore, December 6-10, 2023*, pp. 13512–13525. Association for Computational Linguistics, 2023a. doi: 10.18653/V1/2023.EMNLP-MAIN.833. URL <https://doi.org/10.18653/v1/2023.emnlp-main.833>.
- Chen, L., Huang, H., and Cheng, M. Ptp: Boosting stability and performance of prompt tuning with perturbation-based regularizer. *ArXiv*, abs/2305.02423, 2023b. URL <https://api.semanticscholar.org/CorpusID:258479677>.
- Chen, M., Cao, Y., Zhang, Y., and Lu, C. Quantifying and mitigating unimodal biases in multimodal large language models: A causal perspective. *ArXiv*, abs/2403.18346, 2024a. URL <https://api.semanticscholar.org/CorpusID:268723751>.
- Chen, Z., Wang, W., Cao, Y., Liu, Y., Gao, Z., Cui, E., Zhu, J., Ye, S., Tian, H., Liu, Z., et al. Expanding performance boundaries of open-source multimodal models with model, data, and test-time scaling. *arXiv preprint arXiv:2412.05271*, 2024b.
- Clark, P., Cowhey, I., Etzioni, O., Khot, T., Sabharwal, A., Schoenick, C., and Tafjord, O. Think you have solved question answering? try arc, the ai2 reasoning challenge. *arXiv preprint arXiv:1803.05457*, 2018.
- Contributors, D. Deepspeed. <https://github.com/deepspeedai/DeepSpeed>, 2024. Accessed: 2025-05-14.
- Croce, F. and Hein, M. Reliable evaluation of adversarial robustness with an ensemble of diverse parameter-free attacks. In *Proceedings of the 37th International Conference on Machine Learning, ICML 2020, 13-18 July 2020, Virtual Event*, volume 119 of *Proceedings of Machine Learning Research*, pp. 2206–2216. PMLR, 2020. URL <http://proceedings.mlr.press/v119/croce20b.html>.
- Deka, B., Huang, Z., Franzen, C., Hibsichman, J., Afergan, D., Li, Y., Nichols, J., and Kumar, R. Rico: A mobile app dataset for building data-driven design applications. In *Proceedings of the 30th annual ACM symposium on user interface software and technology*, pp. 845–854, 2017.

- Deng, J., Dong, W., Socher, R., Li, L.-J., Li, K., and Fei-Fei, L. Imagenet: A large-scale hierarchical image database. In *2009 IEEE conference on computer vision and pattern recognition*, pp. 248–255. Ieee, 2009.
- Fei-Fei, L., Fergus, R., and Perona, P. Learning generative visual models from few training examples: An incremental bayesian approach tested on 101 object categories. *2004 Conference on Computer Vision and Pattern Recognition Workshop*, pp. 178–178, 2004. URL <https://api.semanticscholar.org/CorpusID:2156851>.
- Gardner, M., Merrill, W., Dodge, J., Peters, M. E., Ross, A., Singh, S., and Smith, N. A. Competency problems: On finding and removing artifacts in language data. *ArXiv*, abs/2104.08646, 2021. URL <https://api.semanticscholar.org/CorpusID:233296459>.
- Geisler, S., Wollschläger, T., Abdalla, M. H. I., Gasteiger, J., and Günnemann, S. Attacking large language models with projected gradient descent. *CoRR*, abs/2402.09154, 2024. doi: 10.48550/ARXIV.2402.09154. URL <https://doi.org/10.48550/arXiv.2402.09154>.
- Goodfellow, I. J., Shlens, J., and Szegedy, C. Explaining and harnessing adversarial examples. In Bengio, Y. and LeCun, Y. (eds.), *3rd International Conference on Learning Representations, ICLR 2015, San Diego, CA, USA, May 7-9, 2015, Conference Track Proceedings*, 2015. URL <http://arxiv.org/abs/1412.6572>.
- Hendrycks, D., Burns, C., Basart, S., Zou, A., Mazeika, M., Song, D. X., and Steinhardt, J. Measuring massive multi-task language understanding. *ArXiv*, abs/2009.03300, 2020. URL <https://api.semanticscholar.org/CorpusID:221516475>.
- Hosseini, P., Nawathe, S., Moayeri, M., Balasubramanian, S., and Feizi, S. Seeing what’s not there: Spurious correlation in multimodal llms. *ArXiv*, abs/2503.08884, 2025. URL <https://api.semanticscholar.org/CorpusID:276937482>.
- Jaume, G., Ekenel, H. K., and Thiran, J.-P. Funsd: A dataset for form understanding in noisy scanned documents. In *2019 International Conference on Document Analysis and Recognition Workshops (ICDARW)*, volume 2, pp. 1–6. IEEE, 2019.
- Jha, A. and Reddy, C. K. Codeattack: Code-based adversarial attacks for pre-trained programming language models. In Williams, B., Chen, Y., and Neville, J. (eds.), *Thirty-Seventh AAAI Conference on Artificial Intelligence, AAAI 2023, Thirty-Fifth Conference on Innovative Applications of Artificial Intelligence, IAAI 2023, Thirteenth Symposium on Educational Advances in Artificial Intelligence, EAAI 2023, Washington, DC, USA, February 7-14, 2023*, pp. 14892–14900. AAAI Press, 2023. doi: 10.1609/AAAI.V37I12.26739. URL <https://doi.org/10.1609/aaai.v37i12.26739>.
- Jin, D., Jin, Z., Zhou, J. T., and Szolovits, P. Is BERT really robust? A strong baseline for natural language attack on text classification and entailment. In *The Thirty-Fourth AAAI Conference on Artificial Intelligence, AAAI 2020, The Thirty-Second Innovative Applications of Artificial Intelligence Conference, IAAI 2020, The Tenth AAAI Symposium on Educational Advances in Artificial Intelligence, EAAI 2020, New York, NY, USA, February 7-12, 2020*, pp. 8018–8025. AAAI Press, 2020. doi: 10.1609/AAAI.V34I05.6311. URL <https://doi.org/10.1609/aaai.v34i05.6311>.
- Li, B., Wang, R., Wang, G., Ge, Y., Ge, Y., and Shan, Y. Seed-bench: Benchmarking multimodal llms with generative comprehension. *ArXiv*, abs/2307.16125, 2023. URL <https://api.semanticscholar.org/CorpusID:260334888>.
- Lin, J., Yin, H., Ping, W., Molchanov, P., Shoeybi, M., and Han, S. Vila: On pre-training for visual language models. In *Proceedings of the IEEE/CVF conference on computer vision and pattern recognition*, pp. 26689–26699, 2024.
- Liu, H., Li, C., Li, Y., and Lee, Y. J. Improved baselines with visual instruction tuning. *2024 IEEE/CVF Conference on Computer Vision and Pattern Recognition (CVPR)*, pp. 26286–26296, 2023a. URL <https://api.semanticscholar.org/CorpusID:263672058>.
- Liu, H., Li, C., Wu, Q., and Lee, Y. J. Visual instruction tuning. *Advances in neural information processing systems*, 36:34892–34916, 2023b.
- Liu, H., Li, C., Li, Y., and Gao, J. Llava-next: Stronger llms with better visual instruction tuning, 2024. URL <https://llava-vl.github.io/blog/2024-05-10-llava-next-stronger-llms/>.
- Liu, Y., Duan, H., Zhang, Y., Li, B., Zhang, S., Zhao, W., Yuan, Y., Wang, J., He, C., Liu, Z., Chen, K., and Lin, D. Mmbench: Is your multi-modal model an all-around player? In *European Conference on Computer Vision*, 2023c. URL <https://api.semanticscholar.org/CorpusID:259837088>.
- Lu, P., Mishra, S., Xia, T., Qiu, L., Chang, K.-W., Zhu, S.-C., Tafjord, O., Clark, P., and Kalyan, A. Learn to explain: Multimodal reasoning via thought chains for science question answering. *ArXiv*, abs/2209.09513, 2022. URL <https://api.semanticscholar.org/CorpusID:252383606>.

- Luo, Z., Liu, H., Bai, Y., Mu, F., Shi, H., Wang, Z., Yu, J., Lin, X., Wang, Y., Gao, P., Chuang, C., Zeng, M., Zhang, Y. N., and Wang, J. Instructblip: Towards general-purpose vision-language models with instruction tuning. *arXiv preprint arXiv:2305.06500*, 2023.
- Madry, A., Makelov, A., Schmidt, L., Tsipras, D., and Vladu, A. Towards deep learning models resistant to adversarial attacks. In *6th International Conference on Learning Representations, ICLR 2018, Vancouver, BC, Canada, April 30 - May 3, 2018, Conference Track Proceedings*. OpenReview.net, 2018. URL <https://openreview.net/forum?id=rJzIBfZAb>.
- Mihaylov, T., Clark, P., Khot, T., and Sabharwal, A. Can a suit of armor conduct electricity? a new dataset for open book question answering. In *Conference on Empirical Methods in Natural Language Processing*, 2018. URL <https://api.semanticscholar.org/CorpusID:52183757>.
- Oquab, M., Darcet, T., Moutakanni, T., Vo, H., Szafraniec, M., Khalidov, V., Fernandez, P., Haziza, D., Massa, F., El Nouby, A., et al. Dinov2: Learning robust visual features without supervision. *arXiv preprint arXiv:2304.07193*, 2023.
- Pearl, J. Causal diagrams for empirical research. *Biometrika*, 82:669–688, 1995. URL <https://api.semanticscholar.org/CorpusID:10023329>.
- Radford, A., Kim, J. W., Hallacy, C., Ramesh, A., Goh, G., Agarwal, S., Sastry, G., Askell, A., Mishkin, P., Clark, J., Krueger, G., and Sutskever, I. Learning transferable visual models from natural language supervision. In *International Conference on Machine Learning*, 2021. URL <https://api.semanticscholar.org/CorpusID:231591445>.
- Russakovsky, O., Deng, J., Su, H., Krause, J., Satheesh, S., Ma, S., Huang, Z., Karpathy, A., Khosla, A., Bernstein, M., Berg, A. C., and Fei-Fei, L. ImageNet Large Scale Visual Recognition Challenge. *International Journal of Computer Vision (IJCV)*, 115(3):211–252, 2015. doi:10.1007/s11263-015-0816-y.
- Sidorov, O., Hu, R., Rohrbach, M., and Singh, A. Textcaps: a dataset for image captioning with reading comprehension. In *Computer Vision—ECCV 2020: 16th European Conference, Glasgow, UK, August 23–28, 2020, Proceedings, Part II 16*, pp. 742–758. Springer, 2020.
- Singh, A., Natarajan, V., Shah, M., Jiang, Y., Chen, X., Batra, D., Parikh, D., and Rohrbach, M. Towards vqa models that can read. In *Proceedings of the IEEE/CVF conference on computer vision and pattern recognition*, pp. 8317–8326, 2019.
- Tong, S., Liu, Z., Zhai, Y., Ma, Y., LeCun, Y., and Xie, S. Eyes wide shut? exploring the visual shortcomings of multimodal llms. *2024 IEEE/CVF Conference on Computer Vision and Pattern Recognition (CVPR)*, pp. 9568–9578, 2024. URL <https://api.semanticscholar.org/CorpusID:266976992>.
- Wang, F., Zhou, W., Huang, J. Y., Xu, N., Zhang, S., Poon, H., and Chen, M. mdpo: Conditional preference optimization for multimodal large language models. In *Proceedings of the 2024 Conference on Empirical Methods in Natural Language Processing*, pp. 8078–8088, 2024a.
- Wang, P., Bai, S., Tan, S., Wang, S., Fan, Z., Bai, J., Chen, K., Liu, X., Wang, J., Ge, W., et al. Qwen2-vl: Enhancing vision-language model’s perception of the world at any resolution. *arXiv preprint arXiv:2409.12191*, 2024b.
- Wang, W., Lv, Q., Yu, W., Hong, W., Qi, J., Wang, Y., Ji, J., Yang, Z., Zhao, L., Song, X., Xu, J., Xu, B., Li, J., Dong, Y., Ding, M., and Tang, J. Cogvlm: Visual expert for pretrained language models. *ArXiv*, abs/2311.03079, 2023. URL <https://api.semanticscholar.org/CorpusID:265034288>.
- Wei, J., Wang, X., Schuurmans, D., Bosma, M., Xia, F., Chi, E., Le, Q. V., Zhou, D., et al. Chain-of-thought prompting elicits reasoning in large language models. *Advances in neural information processing systems*, 35:24824–24837, 2022.
- Yang, Y., He, X., Pan, H., Jiang, X., Deng, Y., Yang, X., Lu, H., Yin, D., Rao, F., Zhu, M., et al. R1-onevision: Advancing generalized multimodal reasoning through cross-modal formalization. *arXiv preprint arXiv:2503.10615*, 2025.
- Zhang, Y., Unell, A., Wang, X., Ghosh, D., Su, Y., Schmidt, L., and Yeung-Levy, S. Why are visually-grounded language models bad at image classification? *ArXiv*, abs/2405.18415, 2024. URL <https://api.semanticscholar.org/CorpusID:270068069>.
- Zhao, Y., Yin, Y., Li, L., Lin, M., Huang, V. S.-J., Chen, S., Chen, W., Yin, B., Zhou, Z., and Zhang, W. Beyond sight: Towards cognitive alignment in lvlm via enriched visual knowledge. In *Proceedings of the Computer Vision and Pattern Recognition Conference*, pp. 24950–24959, 2025.
- Zhou, G., Yan, Y., Zou, X., Wang, K., Liu, A., and Hu, X. Mitigating modality prior-induced hallucinations in multimodal large language models via deciphering attention causality. In *The Thirteenth International Conference on Learning Representations (ICLR)*, 2025.

Zhu, J., Wang, W., Chen, Z., Liu, Z., Ye, S., Gu, L., Duan, Y., Tian, H., Su, W., Shao, J., et al. Internvl3: Exploring advanced training and test-time recipes for open-source multimodal models. *arXiv preprint arXiv:2504.10479*, 2025.

Zhu, T., Liu, Q., Wang, F., Tu, Z., and Chen, M. Unraveling cross-modality knowledge conflicts in large vision-language models. *ArXiv*, abs/2410.03659, 2024. URL <https://api.semanticscholar.org/CorpusID:273162850>.

## A. Appendix Summary

This appendix provides comprehensive supplementary materials and discussion to support the main findings of our paper on diagnosing and mitigating modality interference in MLLMs. We organize the appendix into several sections:

**Finetuning Strategies** (Section B): We elaborate on our design choice to freeze the Q-Former in InstructBLIP-based models. This decision is motivated by the need to retain strong visual representations while avoiding overfitting to perturbed or misleading multimodal inputs. ( Table 16 records the size for each dataset)

**Detailed Experimental Results** (Section C): This section includes three key tables— Table 5, Table 6 and Table 7—which report model performance on unimodal and multimodal tasks under various perturbation settings and ablation conditions (additional models included). Table 8 records the performance of different vanilla MLLMs under modality interference across modality-heavy datasets. We also include radar plots ( Figure 5) that visualize task-wise robustness across different MLLMs. We provided the detailed experimental results on Qwen2.5-VL-7b (Bai et al., 2025b) and InstructBLIP-Vicuna-13b (Luo et al., 2023) and make further discussion on the selection of specific consistency loss. In Table 12, Table 11, we examine the generalization benefits of adversarial training by evaluating robustness under two types of out-of-distribution (OOD) perturbations: real-world OCR noise (from FUNSD (Jaume et al., 2019)) and unrelated screenshots (from RICO (Deka et al., 2017)) and two new datasets: Food-101 (Bossard et al., 2014) and ARC Challenge (Clark et al., 2018). In Table 9, we assess the impact of Chain-of-Thought prompting in mitigating modality interference, comparing its effectiveness against our method and standard baselines across both visual and textual modalities. In Table 10, we report results on the free-form generative VQA benchmark TextVQA (Singh et al., 2019), highlighting our method’s generalizability beyond multiple-choice formats. In Table 13, we make another ablation study without modality-specific masking.

**Hyperparameter Settings** (Section D): We present full training configurations used in our experiments, including optimization strategies, perturbation settings, and sampling ratios for different task types. This section enables reproducibility and highlights the computational efficiency of our proposed training scheme. We provide parameter analysis on iterations of adversarial training in Figure 6.

**Compute Resource Details** (Section E): We document hardware specifications, training durations, and resource costs for models of different scales. These details contextualize the feasibility of our approach in academic environments.

**Limitations** (Section F): We discuss the granularity of our current modality interference analysis, the selections of per-

turbations, and propose directions for more fine-grained future studies.

**LLM Use** (Section G): Finally, we clarify that LLMs were only used to polish the writing of this paper.

Together, these sections provide a complete view of our technical contributions, empirical findings, and responsible research considerations.

## B. Finetuning Strategies

In our adaptation of InstructBLIP-Vicuna-7B, we choose to freeze the Q-Former and only fine-tune the language model and the projection layer. This decision is grounded in the nature of the Q-Former as a highly task-specific visual query encoder, originally pre-trained on VQA-style datasets where fine-grained and semantically aligned image-text pairs dominate.

However, in our setting, we deliberately introduce perturbations to the input modalities (e.g., injecting unrelated or misleading text/image content), which breaks the expected alignment structure. We observe that training the Q-Former under such noisy supervision leads to unstable representations and overfitting to spurious modality correlations. In contrast, freezing the Q-Former allows us to preserve its original strong visual grounding capabilities, while letting the downstream language model learn to filter or suppress misleading signals introduced during training.

This alternative tuning strategy enhances robustness under modality interference and aligns with our overall goal of improving cross-modal competency in MLLMs under perturbed conditions.

## C. Detailed Experimental Results

Please see Table 5, Table 6, Figure 5, Table 8, Table 7, Table 12, Table 11, Table 9 and Table 10 for more details. In table Table 7: We compare the pretrained models with the following strategies: *FFT with  $D^{VQA}$*  (standard finetuning on VQA data), *FFT with  $D^{AUG}$*  (supervised finetuning on mixed multi-task datasets with heuristic perturbations), *FFT+KL/JS* (adding consistency regularization on KL or JS divergence), *FFT+RG* (injecting random Gaussian noise into token embeddings), *FFT+ADV* (FFT with heuristic & adversarial perturbations), and *Ours* (combining both perturbation-based data augmentation and consistency regularization).

**Diagnosing and Mitigating Modality Interference in Multimodal Large Language Models**

Table 5. Unimodal ability evaluation on image-heavy and text-heavy tasks under perturbation. Left: Mini-ImageNet and Caltech-101; Right: OpenBookQA and MMLU. UF = Unrelated Facts, MD = Misleading Descriptions, RP = Random Pixels, RI = Real Image, FB & FW = Full Black/White Canvas. The best accuracy is marked in bold.

Model	Method	Mini-ImageNet			Caltech-101			OpenBookQA				MMLU			
		Orig	UF	MD	Orig	UF	MD	RP	RI	FB	FW	RP	RI	FB	FW
<b>Qwen2.5-VL-3B</b> <small>(Bai et al., 2025b)</small>	Vanilla	98.9	98.5	94.9	98.8	99.0	94.4	79.9	74.6	80.0	79.7	63.5	61.1	64.0	63.6
	FFT with $D^{VQA}$	98.8	98.5	95.3	98.8	98.1	94.3	<b>80.7</b>	<b>74.3</b>	<b>80.1</b>	80.2	63.0	61.7	63.0	63.3
	FFT with $D^{AUG}$	98.8	98.8	98.6	99.6	99.3	99.6	<b>87.1</b>	<b>86.7</b>	<b>87.4</b>	87.2	64.8	63.9	64.8	64.7
	+ KL	98.9	98.7	99.1	99.6	99.5	<b>99.7</b>	87.1	86.2	86.7	86.8	<b>66.0</b>	<b>65.5</b>	<b>65.9</b>	<b>65.9</b>
	+ JS	99.1	98.8	98.3	99.6	99.4	98.0	85.0	84.2	85.1	85.1	65.6	65.1	65.5	65.5
	+ RG ( $\sigma=0.05$ )	99.0	99.1	98.9	99.5	99.5	99.2	86.4	86.9	86.9	<b>87.2</b>	64.6	64.3	64.6	64.8
	+ ADV	99.3	<b>99.3</b>	99.1	99.5	99.4	99.5	86.6	85.8	86.8	86.6	65.3	64.0	65.4	65.3
Ours	<b>99.3</b>	<b>99.2</b>	<b>99.2</b>	<b>99.7</b>	<b>99.7</b>	99.5	86.7	86.4	86.6	86.6	64.8	64.5	65.0	65.1	
<b>Qwen2.5-VL-7B</b> <small>(Bai et al., 2025b)</small>	Vanilla	99.3	99.3	96.3	99.1	98.9	97.2	85.9	77.5	85.8	86.0	69.3	63.7	68.9	68.9
	FFT with $D^{VQA}$	99.2	99.3	96.0	99.5	99.5	95.7	86.3	82.3	86.5	86.3	69.2	67.4	69.4	69.3
	FFT with $D^{AUG}$	99.6	99.5	99.4	99.7	<b>99.7</b>	99.5	90.2	90.2	90.3	90.3	70.4	69.9	70.4	70.3
	+ KL	99.3	99.3	99.1	99.6	99.6	99.6	<b>92.0</b>	91.7	92.2	92.1	71.2	70.7	71.0	71.0
	+ JS	99.5	99.4	99.4	<b>99.7</b>	99.3	99.6	91.6	92.1	<b>92.2</b>	<b>92.1</b>	<b>71.5</b>	69.9	<b>71.5</b>	<b>71.6</b>
	+ RG ( $\sigma=0.05$ )	99.4	99.4	99.2	99.6	99.3	99.4	89.1	87.9	89.1	89.1	66.7	65.6	66.5	66.5
	+ ADV	99.4	99.3	99.2	99.6	99.5	99.6	91.7	<b>92.2</b>	91.8	91.8	70.4	<b>70.0</b>	70.4	70.4
Ours	<b>99.6</b>	<b>99.5</b>	<b>99.5</b>	99.6	99.6	<b>99.7</b>	90.9	89.7	90.8	91.0	69.8	68.2	69.8	70.0	
<b>LLaVA-1.5-7B</b> <small>(Liu et al., 2023a)</small>	Vanilla	95.3	93.4	43.5	97.0	95.9	57.4	62.4	56.4	62.5	63.4	46.3	45.2	45.9	45.8
	FFT with $D^{VQA}$	94.3	92.7	41.5	96.2	94.0	46.3	61.3	55.5	62.0	62.9	46.8	45.6	47.5	47.7
	FFT with $D^{AUG}$	98.2	98.2	98.1	98.5	98.6	99.0	78.6	77.2	78.7	78.4	51.1	50.7	51.1	51.3
	+ KL	<b>99.1</b>	<b>99.0</b>	98.9	98.6	98.7	98.8	81.4	81.3	81.4	81.2	52.0	51.8	52.0	52.2
	+ JS	98.7	98.8	<b>99.0</b>	99.1	<b>99.0</b>	99.2	81.6	<b>81.6</b>	81.7	81.5	<b>51.6</b>	<b>51.8</b>	<b>52.4</b>	<b>52.4</b>
	+ RG ( $\sigma=0.05$ )	98.4	98.4	98.5	98.9	98.9	99.1	80.5	79.8	79.9	80.3	49.5	49.5	49.9	49.6
	+ ADV	98.7	98.7	98.5	98.7	98.5	98.8	81.7	81.0	81.4	80.8	50.6	50.3	50.9	50.7
Ours	98.6	98.4	98.7	<b>99.3</b>	98.9	<b>99.3</b>	<b>81.8</b>	81.0	<b>81.7</b>	<b>81.7</b>	51.5	50.9	51.5	51.4	
<b>LLaVA-1.5-13B</b> <small>(Liu et al., 2023a)</small>	Vanilla	95.6	94.1	73.0	97.9	97.1	77.4	65.9	63.8	68.0	69.1	51.8	50.8	52.7	52.7
	FFT with $D^{VQA}$	94.6	93.9	72.0	97.8	96.5	80.2	67.5	64.2	69.1	69.3	52.4	52.2	53.1	53.3
	FFT with $D^{AUG}$	98.1	96.8	98.4	96.7	96.9	97.0	81.0	78.7	81.1	81.3	52.1	51.7	51.8	51.6
	+ KL	98.3	98.0	98.6	98.8	98.5	98.9	83.0	82.6	<b>83.3</b>	83.0	55.7	55.1	55.6	55.6
	+ JS	98.3	98.1	98.0	98.7	98.4	98.7	<b>83.1</b>	81.5	83.1	83.1	56.7	<b>56.2</b>	56.6	56.5
	+ RG ( $\sigma=0.05$ )	98.5	98.0s	98.1	98.9	98.5	98.9	83.5	82.5	83.1	82.8	55.4	55.3	55.7	55.5
	+ ADV	<b>98.7</b>	98.2	98.6	99.0	98.6	99.0	82.2	<b>82.6</b>	82.6	82.8	55.6	55.4	55.6	55.5
Ours	98.5	<b>98.4</b>	<b>98.7</b>	<b>99.2</b>	<b>98.6</b>	<b>99.2</b>	83.0	82.1	82.7	<b>83.1</b>	<b>56.7</b>	55.8	<b>56.7</b>	<b>56.7</b>	
<b>InstructBLIP-7B</b> <small>(Luo et al., 2023)</small>	Vanilla	92.0	87.1	13.6	90.3	90.2	17.5	50.8	46.2	50.9	50.7	35.3	35.8	35.2	35.7
	FFT with $D^{VQA}$	95.6	86.6	16.3	98.3	91.0	23.1	49.8	45.2	49.5	50.7	40.9	40.2	41.0	41.6
	FFT with $D^{AUG}$	98.5	98.0	38.2	99.0	98.7	56.1	75.0	74.9	74.8	75.8	50.0	49.7	50.0	50.0
	+ KL	98.7	98.1	<b>98.3</b>	99.5	<b>99.0</b>	<b>99.6</b>	76.9	77.0	76.9	77.3	<b>51.3</b>	<b>50.6</b>	<b>51.3</b>	<b>51.5</b>
	+ JS	98.5	97.7	98.5	98.9	98.4	98.9	78.0	76.6	77.7	78.0	50.7	50.1	50.7	50.8
	+ RG ( $\sigma=0.05$ )	98.9	97.2	72.5	99.1	99.0	82.2	75.2	72.6	76.0	76.9	48.3	47.6	48.9	49.1
	+ ADV	<b>98.7</b>	<b>98.5</b>	32.2	<b>99.5</b>	98.9	49.2	76.8	76.8	76.5	76.3	49.3	48.4	49.5	49.4
Ours	98.4	97.9	98.0	99.2	98.3	99.0	<b>79.0</b>	<b>77.3</b>	<b>79.3</b>	<b>79.0</b>	50.2	49.7	50.3	50.2	
<b>InstructBLIP-13B</b> <small>(Luo et al., 2023)</small>	Vanilla	95.6	94.1	73.0	97.9	97.1	77.4	65.9	63.8	68.0	69.1	51.8	50.8	52.7	52.7
	FFT with $D^{VQA}$	95.6	85.8	8.0	97.0	87.5	11.6	58.6	55.4	59.7	60.6	43.7	42.8	43.6	44.1
	FFT with $D^{AUG}$	98.4	98.2	9.3	99.2	98.8	13.8	82.0	80.4	81.2	81.2	52.1	51.3	52.4	53.0
	+ KL	98.5	<b>98.3</b>	98.7	99.1	99.2	99.5	82.5	81.4	82.1	82.9	<b>53.4</b>	<b>52.5</b>	<b>53.4</b>	53.4
	+ JS	98.7	98.1	<b>98.9</b>	99.3	99.2	<b>99.5</b>	<b>83.5</b>	<b>83.1</b>	83.1	<b>83.3</b>	52.8	52.2	53.2	53.3
	+ RG ( $\sigma=0.05$ )	98.4	97.8	87.0	<b>99.4</b>	<b>99.3</b>	94.4	80.0	76.6	79.6	80.4	50.9	50.0	51.4	51.8
	+ ADV	98.6	98.0	80.9	98.7	98.6	99.1	79.8	79.0	80.9	80.9	51.3	50.7	51.4	52.4
Ours	<b>98.7</b>	97.9	98.0	98.7	98.7	98.8	83.2	81.2	<b>83.8</b>	83.0	52.2	51.6	52.3	<b>53.4</b>	

**Diagnosing and Mitigating Modality Interference in Multimodal Large Language Models**

Table 6. Evaluation of unimodal and multimodal tasks across different ablation study settings. For unimodal datasets, we report accuracy on the original setting (Orig) and the worst-performing perturbation (Perturbed). For VQA datasets, we report accuracy on the original setting. The best accuracy is marked in bold.

Model	Method	Mini-ImageNet		Caltech-101		OpenBookQA		MMLU		VQA Overall Accuracy
		Orig	Perturbed	Orig	Perturbed	Orig	Perturbed	Orig	Perturbed	
<b>3B Multimodal Models</b>										
<b>Qwen2.5-VL-3B</b> <small>(Bai et al., 2025b)</small>	Vanilla	98.9	94.9	98.8	94.4	79.9	74.6	63.5	61.1	72.5
	FFT with $D^{VQA}$	98.8	95.3	98.8	94.3	80.7	74.3	63.0	61.7	75.5
	FFT with $D^{AUG}$	98.8	98.6	99.6	99.3	87.1	86.2	64.8	63.9	76.2
	+ KL	98.9	98.7	99.6	99.5	<b>87.1</b>	<b>86.7</b>	<b>66.0</b>	<b>65.5</b>	75.9
	+ JS	99.1	98.3	99.6	98.0	85.0	84.2	65.6	65.1	76.2
	+ RG	99.0	98.9	99.5	99.2	86.4	86.4	64.6	64.3	76.0
	+ ADV	99.3	99.1	99.5	99.4	86.6	85.8	65.3	64	76.1
	Ours	<b>99.3</b>	<b>99.2</b>	<b>99.7</b>	<b>99.5</b>	86.7	86.6	64.8	64.5	<b>76.4</b>
<b>7B Multimodal Models</b>										
<b>LLaVA-1.5-7B</b> <small>(Liu et al., 2023a)</small>	Vanilla	95.3	43.5	97.0	57.4	62.4	56.4	46.3	45.2	63.8
	FFT with $D^{VQA}$	94.3	41.5	96.2	46.3	61.3	55.5	46.8	45.6	64.0
	FFT with $D^{AUG}$	98.2	98.1	98.5	98.6	78.6	77.2	51.1	50.7	65.6
	+ KL	<b>99.1</b>	<b>99.0</b>	98.6	98.7	81.4	81.2	51.1	50.7	66.3
	+ JS	98.7	98.8	99.1	99.0	81.6	81.5	<b>52.0</b>	<b>51.8</b>	65.6
	+ RG	98.4	98.4	98.9	98.9	80.5	79.8	49.5	49.5	65.7
	+ ADV	98.7	98.5	98.7	98.5	81.7	80.8	50.6	50.3	65.7
	Ours	98.6	98.6	<b>99.3</b>	<b>99.0</b>	<b>81.8</b>	<b>81.5</b>	51.5	51.0	<b>66.8</b>
<b>InstructBLIP-7B</b> <small>(Luo et al., 2023)</small>	Vanilla	92.0	13.6	90.3	17.5	50.9	46.2	35.3	35.2	56.4
	FFT with $D^{VQA}$	95.6	16.3	98.3	23.1	49.8	45.2	40.9	40.2	60.4
	FFT with $D^{AUG}$	98.5	38.2	99.0	56.1	75.0	74.8	50.0	49.7	63.9
	+ KL	98.7	<b>98.1</b>	99.5	<b>99.0</b>	76.9	76.9	<b>51.3</b>	<b>50.6</b>	63.9
	+ JS	98.5	97.7	98.9	98.4	78.0	76.6	50.7	50.1	64.1
	+ RG	<b>98.9</b>	72.5	99.1	82.2	76.0	72.6	48.3	47.6	64.2
	+ ADV	98.7	72.2	<b>99.5</b>	85.2	76.8	76.3	49.3	48.4	64.0
	Ours	98.4	98.0	99.2	98.3	<b>79.0</b>	<b>78.3</b>	50.2	49.7	<b>64.8</b>
<b>Qwen2.5-VL-7B</b> <small>(Luo et al., 2023)</small>	Vanilla	99.3	96.3	99.1	97.2	85.9	77.5	69.3	63.7	80.3
	FFT with $D^{VQA}$	99.2	96.0	99.5	95.7	86.3	82.3	69.2	67.4	79.5
	FFT with $D^{AUG}$	99.6	99.4	<b>99.7</b>	99.5	90.2	90.2	70.4	69.9	79.9
	+ KL	99.3	99.1	99.6	99.6	<b>92.0</b>	91.7	71.2	<b>70.7</b>	80.6
	+ JS	99.5	99.4	99.7	99.3	91.6	<b>92.1</b>	<b>71.5</b>	69.9	80.3
	+ RG	99.4	99.3	99.7	99.5	91.7	91.8	70.4	69.9	78.0
	+ ADV	99.4	99.2	99.6	99.5	91.7	91.8	70.4	70.0	79.9
	Ours	<b>99.6</b>	<b>99.5</b>	99.6	<b>99.7</b>	90.9	89.7	69.8	68.2	<b>80.9</b>
<b>13B Multimodal Models</b>										
<b>LLaVA-1.5-13B</b> <small>(Liu et al., 2023a)</small>	Vanilla	95.6	73.0	97.9	77.4	65.9	63.8	51.8	50.8	66.2
	FFT with $D^{VQA}$	94.6	72.0	97.8	80.2	67.5	64.2	52.4	52.2	65.8
	FFT with $D^{AUG}$	98.1	96.8	96.7	96.9	81.0	78.7	52.1	51.6	67.1
	+ KL	98.3	98.0	98.8	98.5	83.0	<b>82.6</b>	55.7	55.1	68.0
	+ JS	98.3	98.1	98.7	98.4	83.1	81.5	56.7	<b>56.2</b>	<b>68.6</b>
	+ RG	98.5	98.0	98.9	98.5	<b>83.5</b>	82.5	55.4	55.3	66.9
	+ ADV	<b>98.7</b>	98.2	99.0	98.6	82.2	82.5	55.6	55.4	67.5
	Ours	98.5	<b>98.4</b>	<b>99.2</b>	<b>98.7</b>	83.0	82.1	<b>56.7</b>	56.0	68.4
<b>InstructBLIP-13B</b> <small>(Luo et al., 2023)</small>	Vanilla	95.6	73.0	97.9	77.4	65.9	63.8	51.8	50.8	65.8
	FFT with $D^{VQA}$	95.6	8.0	97.0	11.6	58.6	55.4	43.7	42.8	59.4
	FFT with $D^{AUG}$	98.4	9.3	99.2	13.8	82.0	80.4	52.1	51.3	65.9
	+ KL	98.5	<b>98.3</b>	99.1	99.2	82.5	81.4	<b>53.4</b>	<b>52.5</b>	66.2
	+ JS	98.7	98.1	99.3	99.2	<b>83.5</b>	<b>83.1</b>	52.8	52.2	66.5
	+ RG	98.4	97.8	<b>99.4</b>	<b>99.3</b>	80.0	76.6	50.9	50.0	66.3
	+ ADV	98.6	80.9	98.7	98.6	79.8	79.0	51.3	50.7	66.4
	Ours	<b>98.7</b>	97.9	98.7	98.7	83.2	81.2	52.2	51.6	<b>66.5</b>

**Diagnosing and Mitigating Modality Interference in Multimodal Large Language Models**

Table 7. Detailed multimodal reasoning accuracy (%) on multiple-choice VQA datasets across different ablation study settings with extra models: Qwen2.5-vl-7B, Instructblip-Vicuna-13B. The best accuracy is marked in bold. Overall performance is computed as a weighted average across datasets, with weights proportional to each dataset’s test size.

Model	Method	ScienceQA-IMG	MM-Bench-EN	Seed-Bench-IMG	VQA Overall
<i>Qwen2.5-VL Models (Bai et al., 2025b)</i>					
<b>Qwen2.5-VL-3B</b> (Bai et al., 2025b)	Vanilla	63.0 (100%)	81.8 (100%)	72.3 (100%)	72.5 (100%)
	FFT with $D^{VQA}$	72.2 (↑14.6%)	82.0 (↑0.2%)	74.7 (↑3.3%)	75.5 (↑3.9%)
	FFT with $D^{AUG}$	73.6 (↑16.8%)	81.7 (↓0.1%)	75.3 (↑4.1%)	76.2 (↑5.1%)
	+ KL	72.8 (↑15.6%)	80.9 (↓1.1%)	74.9 (↑3.6%)	75.9 (↑4.7%)
	+ JS	73.4 (↑16.5%)	82.0 (↑0.2%)	75.2 (↑4.0%)	76.2 (↑5.1%)
	+ RG	73.4 (↑16.5%)	81.8 (↑0.0%)	75.0 (↑3.7%)	76.0 (↑4.8%)
	+ ADV	73.1 (↑16.0%)	81.7 (↓0.1%)	75.3 (↑4.1%)	76.1 (↑5.0%)
	Ours	73.8 (↑17.1%)	82.1 (↑0.1 %)	75.5 (↑4.4%)	<b>76.4 (↑5.4%)</b>
<b>Qwen2.5-VL-7B</b> (Bai et al., 2025b)	Vanilla	85.1 (100%)	86.6 (100%)	77.0 (100%)	80.3 (100%)
	FFT with $D^{VQA}$	81.4 (↓4.3%)	86.4 (↓0.2%)	76.8 (↓0.3%)	79.5 (↓1.0%)
	FFT with $D^{AUG}$	83.2 (↓2.2%)	86.1 (↓0.6%)	77.0 (-0.0%)	79.9 (↓0.5%)
	+ KL	86.0 (↑1.1%)	86.7 (↑0.1%)	77.2 (↑0.3%)	80.6 (↑0.4%)
	+ JS	85.5 (↑0.5%)	85.9 (↓0.8%)	77.0 (-0.0%)	80.3 (-0.0%)
	+ RG	81.6 (↓4.1%)	82.9 (↓4.2%)	75.5 (↓1.9%)	78.0 (↓2.8%)
	+ ADV	85.2 (↑0.1%)	85.8 (↓0.9%)	76.6 (↓0.5%)	79.9 (↓0.5%)
	Ours	83.9 (↓1.4%)	86.4 (↓0.2%)	78.3 (↑1.7%)	<b>80.9 (↑0.7%)</b>
<i>Instructblip-Vicuna Models (Luo et al., 2023)</i>					
<b>InstructBLIP-7B</b> (Luo et al., 2023)	Vanilla	52.1 (100%)	65.5 (100%)	54.8 (100%)	56.4 (100%)
	FFT with $D^{VQA}$	61.8 (↑18.6%)	68.4 (↑4.4%)	57.6 (↑5.1%)	60.4 (↑7.1%)
	FFT with $D^{AUG}$	65.4 (↑25.5%)	71.1 (↑8.5%)	61.2 (↑11.7%)	63.9 (↑13.3%)
	+ KL	65.9 (↑26.5%)	71.7 (↑9.5%)	60.9 (↑11.1%)	63.9 (↑13.3%)
	+ JS	66.9 (↑28.4%)	72.3 (↑10.4%)	60.7 (↑10.8%)	64.1 (↑13.7%)
	+ RG	62.8 (↑20.5%)	70.9 (↑8.2%)	62.5 (↑14.0%)	64.2 (↑13.8%)
	+ ADV	66.0 (↑26.7%)	69.0 (↑5.3%)	61.8 (↑12.8%)	64.0 (↑13.5%)
	Ours	64.0 (↑22.8%)	71.4 (↑9.0%)	63.0 (↑14.9%)	<b>64.8 (↑14.9%)</b>
<b>InstructBLIP-13B</b> (Luo et al., 2023)	Vanilla	65.8 (100%)	72.1 (100%)	63.8 (100%)	65.8 (100%)
	FFT with $D^{VQA}$	61.7 (↓6.2%)	68.5 (↓5.0%)	56.0 (↓12.2%)	59.4 (↓9.7%)
	FFT with $D^{AUG}$	66.6 (↑1.2%)	71.5 (↓0.8%)	64.0 (↑0.3%)	65.9 (↑0.2%)
	+ KL	67.2 (↑2.2%)	72.6 (↑0.7%)	64.0 (↑0.3%)	66.2 (↑0.6%)
	+ JS	67.9 (↑3.2%)	72.7 (↑0.8%)	64.2 (↑0.6%)	66.5 (↑1.1%)
	+ RG	65.4 (↓0.6%)	73.5 (↑1.9%)	64.3 (↑0.7%)	66.3 (↑0.8%)
	+ ADV	66.1 (↑0.5%)	74.0 (↑2.6%)	64.1 (↑0.5%)	66.4 (↑0.9%)
	Ours	66.2 (↑0.6%)	73.2 (↑1.5%)	64.3 (↑0.7%)	<b>66.5 (↑1.1%)</b>
<i>LLaVA1.5 Models (Liu et al., 2023a)</i>					
<b>LLaVA-1.5-7B</b> (Liu et al., 2023a)	Vanilla	64.5 (100%)	64.3 (100%)	63.4 (100%)	63.8 (100%)
	FFT with $D^{VQA}$	61.6 (↓4.5%)	71.4 (↑11.0%)	62.4 (↓1.6%)	64.0 (↑0.3%)
	FFT with $D^{AUG}$	65.4 (↑1.4%)	71.1 (↑10.6%)	63.9 (↑0.8%)	65.6 (↑2.8%)
	+ KL	65.9 (↑2.2%)	72.5 (↑12.8%)	64.5 (↑1.7%)	66.3 (↑3.9%)
	+ JS	63.8 (↓1.1%)	73.5 (↑14.3%)	63.7 (↑0.5%)	65.6 (↑2.8%)
	+ RG	66.3 (↑2.8%)	71.8 (↑11.7%)	63.7 (↑0.5%)	65.7 (↑3.0%)
	+ ADV	66.7 (↑3.4%)	71.4 (↑11.0%)	63.6 (↑0.3%)	65.7 (↑3.0%)
	Ours	67.8 (↑5.1%)	73.1 (↑13.7%)	64.6 (↑1.9%)	<b>66.8 (↑4.7%)</b>
<b>LLaVA-1.5-13B</b> (Liu et al., 2023a)	Vanilla	65.8 (100%)	72.1 (100%)	64.5 (100%)	66.2 (100%)
	FFT with $D^{VQA}$	60.8 (↓7.6%)	73.6 (↑2.1%)	64.9 (↑0.6%)	65.8 (↓0.6%)
	FFT with $D^{AUG}$	63.5 (↓3.5%)	75.0 (↑4.0%)	65.7 (↑1.9%)	67.1 (↑1.4%)
	+ KL	62.5 (↓5.0%)	74.6 (↑3.5%)	67.6 (↑4.8%)	68.0 (↑2.7%)
	+ JS	65.8 (↑0.0%)	74.7 (↑3.6%)	67.6 (↑4.8%)	68.6 (↑3.6%)
	+ RG	58.3 (↓11.4%)	73.5 (↑1.9%)	67.4 (↑4.5%)	66.9 (↑1.1%)
	+ ADV	57.6 (↓12.5%)	74.2 (↑2.9%)	68.3 (↑5.9%)	67.5 (↑2.0%)
	Ours	62.6 (↓4.9%)	73.7 (↑2.2%)	68.4 (↑6.0%)	<b>68.4 (↑3.3%)</b>

Note. While Qwen2.5-VL was originally instruction-tuned with proprietary in-house data (Bai et al., 2025b), our reproduced version uses only publicly available LLaVA instruction-tuning data. Even under this constraint and without access to VQA-specific tuning samples, our models achieve comparable or even better performance across all VQA datasets—highlighting the robustness and effectiveness of our proposed perturbation-consistent fine-tuning strategy.

### C.1. Perturbation-based Evaluation Experiment Results

We conduct a controlled perturbation-based evaluation across various MLLMs, as shown in Table 8. Our results reveal that both vision and language tasks are vulnerable to cross-modal interference. In vision classification tasks, misleading textual descriptions (e.g., text contradicting image content) lead to severe performance drops. For example, InternVL2-2B and InstructBLIP-7B on Mini-ImageNet drop from 91.9% to 25.5% and from 92.0% to 13.6%, respectively. Conversely, for language tasks such as OpenBookQA and MMLU, irrelevant visual inputs—particularly semantically unrelated real images—also degrade performance. LLaVA-1.5-7B drops from 46.3% to 45.2% on MMLU, while InstructBLIP-13B sees over 5 points of degradation.

A consistent trend is that larger models exhibit greater robustness. Models like LLaVA-1.5-13B and QwenVL2.5-7B maintain high accuracy across all perturbation types—e.g., QwenVL2.5-7B sustains over 96% on Mini-ImageNet with misleading text and over 86% on OpenBookQA with irrelevant images—indicating improved modality disentanglement and reduced sensitivity to spurious correlations. Nonetheless, performance still degrades relative to clean inputs, highlighting that interference effects remain non-negligible even in stronger models.

We further observe a clear scaling trend within the LLaVA-Next family. As model size increases from 7B to 34B, 72B, and 110B, performance under perturbations steadily improves, reflecting stronger representation power and enhanced robustness to spurious cues. For instance, LLaVA-Next-7B achieves 90.3% on Mini-ImageNet (Orig) but drops to 28.5% with misleading descriptions, whereas LLaVA-Next-110B maintains 98.4% and 93.3% under the same conditions. Similarly, on MMLU, accuracy under irrelevant real images increases from 45.9% (7B) to 73.6% (72B). **These results confirm that scaling up helps mitigate modality interference. However, such gains come at substantial computational and resource costs, and the improvements remain incremental relative to the clean-perturbed gap.** This underscores that scaling alone is insufficient, and more targeted interventions—such as our proposed framework—are necessary for robust cross-modal reasoning.

### C.2. Experiment Results on InstructBLIP-Vicuna-13b and QwenVL-2.5-7b

To enable a more equitable comparison with existing multimodal models, we extend our method to two additional backbones: InstructBLIP-Vicuna-13B and QwenVL-2.5-7B. As shown in Table 7, our approach consistently improves performance across multiple VQA benchmarks, even under different instruction-tuning conditions, demonstrating its robustness and general applicability.

### C.3. Discussion on KL&JS use for Consistency Regularization

Although both KL and JS divergence serve as effective objectives for consistency regularization, we find that JS consistently achieves slightly better results across most settings. Specifically, in both unimodal tasks (e.g., Mini-ImageNet, MMLU) and multimodal reasoning benchmarks (e.g., ScienceQA, SeedBench), JS-regularized models consistently outperform their KL counterparts by a small but observable margin. This trend holds across different model backbones and training configurations, including our final unified method (see “Ours” rows in Table 5 and 7). This suggests a marginal advantage of JS regularization in enhancing model robustness.

### C.4. Evaluating Chain-of-Thought Prompting for Modality Interference Mitigation

To further investigate the potential of prompt-based methods in mitigating modality interference, we conduct additional experiments using Chain-of-Thought (Wei et al., 2022) style prompting. This approach aims to encourage structured reasoning by guiding the model through an explicit reasoning process before producing its final answer.

Specifically, we prepend the following CoT prompt to each input question:

```
Let's think step by step:
1. What information does the image provide?
2. What is the question asking?
3. Are there any misleading parts?
4. Now give your final answer.
Only write the final answer on a separate line like: ``Answer: B''
```

Results are presented in Table 9. The results suggests that structured reasoning alone cannot resolve the interference problem, as the issue stems from misaligned cross-modal representations rather than shallow reasoning steps.

### C.5. Evaluation on Free-Form VQA

To further assess the generalizability of our method beyond multiple-choice VQA tasks, we evaluate on TextVQA (Singh et al., 2019), a free-form generative visual question answering dataset that requires reasoning over both textual and visual content in natural images. We follow the benchmark adopted by LLaVA (Liu et al., 2023b), which evaluates a model’s ability to both recognize textual characters within images and effectively handle noisy outputs generated by OCR systems.

Following standard evaluation protocols and existing MLLM baselines (e.g., LLaVA, Qwen2.5-VL, InstructBLIP), we report model performance averaged over multiple

## Diagnosing and Mitigating Modality Interference in Multimodal Large Language Models

Table 8. Performance (%) of V a lin na models under modality interference across four datasets. We show accuracy under clean (origin) and various perturbations: Left: Mini-ImageNet and Caltech-101; Right: OpenBookQA and MMLU. UF = Unrelated Facts, MD = Misleading Descriptions, RP = Random Pixels, RI = Real Image, FB & FW = Full Black/White Canvas. (The results are averaged on multiple runs with standard deviation < 0.2)

Model	Mini-ImageNet			Caltech-101			Open-Book QA				MMLU			
	Orig	UF	MD	Orig	UF	MD	RP	RI	FB	FW	RP	RI	FB	FW
InternVL2-2B (Chen et al., 2024b)	91.9	88.6	25.5	94.6	91.3	33.2	46.3	36.2	45.2	45.3	39.1	36.9	39.3	39.2
LLaVA-1.5-7B (Liu et al., 2023a)	95.3	93.4	43.5	97.0	95.9	57.4	62.4	56.4	62.5	63.4	46.3	45.2	45.9	45.8
LLaVA-Next-7B (Liu et al., 2024)	93.4	90.0	28.5	97.0	93.4	31.6	54.6	52.9	55.9	55.5	45.9	45.0	45.9	45.8
LLaVA-Next-34B (Liu et al., 2024)	98.0	96.3	90.2	99.1	97.3	93.6	87.7	85.7	88.4	88.0	71.5	70.9	71.5	71.5
LLaVA-Next-72B (Liu et al., 2024)	97.7	97.8	83.0	98.9	98.8	91.2	88.2	86.2	89.1	88.9	73.6	72.9	73.9	73.9
LLaVA-Next-110B (Liu et al., 2024)	98.4	98.3	93.3	98.4	98.3	93.1	89.5	89.2	89.9	89.7	73.5	73.0	73.9	73.9
LLaVA-1.5-13B (Liu et al., 2023a)	95.6	94.1	73.0	97.9	97.1	77.4	65.9	63.8	68.0	69.1	51.8	50.8	52.7	52.7
InstructBLIP-7B (Luo et al., 2023)	92.0	87.1	13.6	90.3	90.2	17.5	50.8	46.2	50.9	50.7	36.3	35.2	36.2	36.7
InstructBLIP-13B (Luo et al., 2023)	93.0	81.6	50.9	94.1	82.7	51.0	44.7	39.4	45.6	46.1	40.1	37.4	40.5	42.9
QwenVL2-2B (Wang et al., 2024b)	98.7	98.6	75.8	99.1	99.1	66.8	59.6	54.7	63.4	63.8	49.5	44.6	49.7	50.0
QwenVL2.5-3B (Bai et al., 2025b)	98.9	98.5	94.9	98.8	99.0	94.4	79.9	74.6	80.0	79.7	63.5	61.1	64.0	63.6
QwenVL3-4B (Bai et al., 2025a)	99.6	99.1	96.4	99.3	99.2	98.0	84	82.3	86.7	86.4	71.8	70.9	72.4	72.4
QwenVL2-7B (Wang et al., 2024b)	99.0	99.1	96.3	99.6	99.5	97.6	82.5	80.9	83.7	83.2	66.9	65.3	67.7	67.8
QwenVL2.5-7B (Bai et al., 2025b)	99.3	99.3	96.5	99.3	99.4	96.8	86.2	80.9	86.3	86.4	69.5	67.6	69.1	69.1
QwenVL3-8B (Bai et al., 2025a)	99.3	98.8	97.2	99.8	99.7	98.1	87.0	85.7	87.5	88.1	75.6	75.0	76.2	76.3

Table 9. Accuracy (%) under different interference settings across tasks and models. Each task includes original inputs and multiple types of perturbations.

Model	Method	Mini-ImageNet			Caltech-101			OpenBookQA				MMLU			
		Orig	UF	MD	Orig	UF	MD	RP	RI	FB	FW	RP	RI	FB	FW
vanilla	llava-1.5-7b	95.3	93.4	43.5	97.0	95.9	57.4	62.4	56.4	62.5	63.4	46.3	45.2	45.9	45.8
CoT	llava-1.5-7b	81.7	70.9	28.9	80.9	71.8	36.0	38.8	38.9	41.0	41.0	39.6	38.7	40.2	40.4
Ours	llava-1.5-7b	98.6	98.4	98.7	99.3	98.9	99.3	81.8	81.0	81.7	81.7	51.5	50.9	51.5	51.4
vanilla	llava-1.5-13b	95.6	94.1	73.0	97.9	97.1	77.4	65.9	63.8	68.0	69.1	51.8	50.8	52.7	52.7
CoT	llava-1.5-13b	92.9	85.9	62.8	96.6	92.1	67.8	55.6	53.0	56.5	57.3	47.3	45.5	47.3	47.8
Ours	llava-1.5-13b	98.7	97.9	98.0	98.7	98.7	98.8	83.2	81.2	83.8	83.0	52.2	51.6	52.3	53.4
vanilla	qwen2.5-vl-3b	98.9	98.5	94.9	98.8	99.0	94.4	79.9	74.6	80.0	79.7	63.5	61.1	64.0	63.6
CoT	qwen2.5-vl-3b	92.3	96.8	88.2	94.7	96.1	86.0	61.0	52.8	61.3	61.1	51.5	48.7	51.6	51.4
Ours	qwen2.5-vl-3b	99.3	99.2	99.2	99.7	99.7	99.5	86.7	86.4	86.6	86.6	64.8	64.5	65.0	65.1
vanilla	qwen2.5-vl-7b	99.3	99.3	96.3	99.1	98.9	97.2	85.9	77.5	85.8	86.0	69.3	63.7	68.9	68.9
CoT	qwen2.5-vl-7b	99.1	98.9	91.4	98.5	98.5	92.5	77.8	68.8	77.3	77.6	61.5	57.4	60.8	60.9
Ours	qwen2.5-vl-7b	99.6	99.5	99.5	99.6	99.6	99.7	90.9	89.7	90.8	91.0	69.8	68.2	69.8	70.0

runs (standard deviation < 0.4). Results are presented in Table 10.

Our method achieves consistent improvements across most model families, indicating its effectiveness not only in MCQA scenarios but also in open-ended multimodal reasoning settings.

### C.6. Improving Generalizability through Adversarial Training

To assess the generalization benefits of adversarial training, we evaluate model robustness under two types of out-of-distribution (OOD) perturbations at test time:

- **Document OCR noise:** Real-world noisy OCR snip-

Table 10. Accuracy (%) on the TextVQA dataset across different model families.

Setting	Model	TextVQA
Vanilla	InstructBLIP-Vicuna-7B	19.7
Ours	InstructBLIP-Vicuna-7B	<b>32.4</b>
Vanilla	LLaVA-1.5-7B	49.8
Ours	LLaVA-1.5-7B	<b>51.2</b>
Vanilla	Qwen2.5-VL-7B	81.4
Ours	Qwen2.5-VL-7B	<b>84.8</b>

pets are sampled from the FUNSD dataset (Jaume et al., 2019) and inserted as irrelevant textual distractors into image-heavy visual classification tasks (Mini-

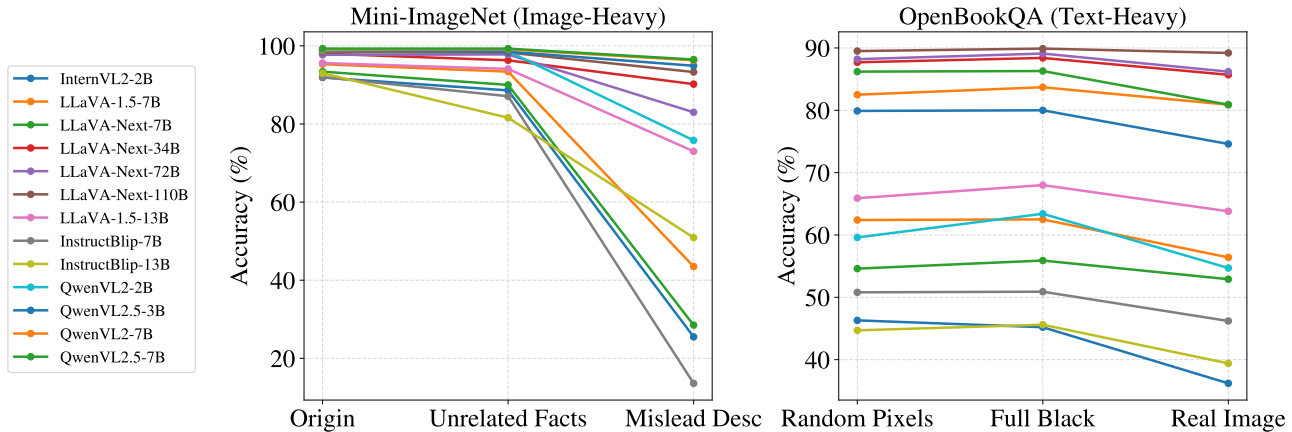


Figure 4. Performance degradation under irrelevant perturbations reveals modality interference in MLLMs. Left: Mini-ImageNet (image-heavy) with Original input, Unrelated Facts, and Misleading Descriptions. Right: OpenBookQA (text-heavy) with Random Pixels, Full Black Canvas, and Irrelevant Real Images. Misleading descriptions most severely affect image-heavy tasks, while irrelevant real images cause the largest drop in text-heavy reasoning.

ImageNet, Caltech-101).

- **Unrelated screenshots:** Unrelated UI screenshots are drawn from the RICO dataset (Deka et al., 2017) and added as visual distractors to text-heavy reasoning tasks (OpenBookQA, MMLU).

Beyond these seen datasets, we further evaluate generalization on two *completely unseen datasets* at test time: **Food-101** and **ARC Challenge**. Food-101 serves as an unseen image-heavy classification benchmark, where models are exposed to diverse textual perturbations, including unrelated descriptions, misleading class cues, and OCR-style noise. ARC Challenge represents an unseen text-heavy reasoning task, where various visual distractors—such as random pixels, unrelated real images, full-black/white images, and UI screenshots—are introduced to probe robustness against spurious visual signals.

Each experiment is repeated multiple times, and we report average accuracy across runs (standard deviation  $< 0.1$ ). Results on seen datasets are presented in Table Table 11, while results on unseen datasets are summarized in Table 12. Across all model families and task types, adversarial training consistently improves robustness to both unseen perturbation types and unseen datasets. In contrast, heuristic data augmentation alone often fails to generalize beyond the perturbation patterns observed during training and can even degrade performance under novel noise.

Overall, these results demonstrate that adversarial training substantially enhances out-of-domain generalization with only modest additional training overhead. This improved robustness to distribution shifts is crucial for reliable deployment of multimodal models in real-world, noisy environments.

### C.7. Ablation without Modality Mask

To further examine the role of modality-aware masking, we implement a *No Mask* variant, where adversarial perturbations are applied uniformly to all modalities across all datasets, including VQA tasks.

Table 13 reports the results on representative image-heavy and text-heavy benchmarks. We observe three key findings. First, training without a modality mask still partially mitigates modality interference. This is because the combination of consistency regularization and heuristic perturbations already encourages the model to learn certain modality-invariant features, and adversarial training itself improves generic robustness (e.g., on OpenBookQA with screenshot distractors, accuracy improves from 50.2% to 62.7%).

Second, the modality mask is critical for out-of-distribution generalization. Without masking, performance collapses on unseen perturbations, particularly under strong visual distractions. For example, on OpenBookQA with screenshot perturbations, the No Mask variant underperforms the masked version by a large margin (62.7% vs. 81.8%).

Third, modality-aware masking is essential to preserve multimodal semantics during VQA training. When adversarial noise is injected into all token embeddings indiscriminately, the model fails to maintain coherent cross-modal representations, resulting in a notable degradation in overall VQA performance (61.5% vs. 66.8%).

Together, these results demonstrate that while adversarial training alone improves robustness, modality-aware masking plays a crucial role in preventing semantic destruction and enabling reliable generalization under unseen distribution shifts.

Table 11. Accuracy (%) on original and perturbed inputs. OCR snippets are inserted into image classification tasks, and RICO screenshots are added to VQA tasks.

Setting	Model	Mini-ImageNet		Caltech-101		OpenBookQA		MMLU	
		Origin	OCR	Origin	OCR	RandPixels	Screenshot	RandPixels	Screenshot
vanilla	instructblip-vicuna-7b	92.0	81.4	90.3	83.6	50.9	40.0	35.3	34.9
SFT	instructblip-vicuna-7b	98.5	95.7	99.0	98.4	75.0	74.4	50.0	49.2
SFT + ADV	instructblip-vicuna-7b	98.7	97.5	99.5	98.8	76.8	76.2	49.3	49.3
Ours	instructblip-vicuna-7b	98.4	97.3	99.2	99.0	79.0	77.8	50.2	49.2
vanilla	llava-1.5-7b	95.3	88.9	97.0	92.8	62.4	50.2	46.3	44.8
SFT	llava-1.5-7b	98.2	98.0	98.5	98.0	78.6	78.0	51.1	50.6
SFT + ADV	llava-1.5-7b	98.7	98.2	98.7	98.4	81.7	81.3	50.6	51.3
Ours	llava-1.5-7b	98.6	98.2	99.3	99.0	81.8	81.2	51.5	51.3
vanilla	qwen2.5-vl-7b	99.3	99.2	99.1	99.2	85.9	69.3	69.3	57.0
SFT	qwen2.5-vl-7b	99.6	99.5	99.7	99.3	90.2	85.8	70.4	63.7
SFT + ADV	qwen2.5-vl-7b	99.4	99.5	99.6	99.6	91.7	91.5	70.4	69.7
Ours	qwen2.5-vl-7b	99.6	99.5	99.6	99.5	90.9	90.7	69.8	69.7

Table 12. Accuracy (%) on Food-101 (image-heavy) and ARC Challenge (text-heavy) under diverse test-time perturbations. For Food-101, we add different types of textual distractors (unrelated, misleading, and OCR-style noise). For ARC Challenge, we use various visual distractors (random pixels, unrelated real images, full-black/white images, and UI screenshots).

Setting	Model	Food-101				ARC Challenge				
		Origin	Unrelated Text	Mislead Text	OCR Text	RandPixels	Real Image	Full Black	Full White	Screenshot
vanilla	qwen2.5-vl-7b	97.1	96.8	93.3	96.7	85.6	83.7	85.9	85.9	79.6
+D <sup>AUG</sup>	qwen2.5-vl-7b	97.1	96.6	94.1	96.5	85.0	82.9	84.9	84.9	80.2
Ours	qwen2.5-vl-7b	97.5	97.5	97.6	97.4	84.1	82.7	84.2	84.0	82.6
vanilla	llava-1.5-7b	90.2	86.3	31.0	83.6	53.4	51.6	54.5	54.0	51.8
+D <sup>AUG</sup>	llava-1.5-7b	91.3	86.5	40.2	83.5	55.7	52.0	56.0	56.0	53.8
Ours	llava-1.5-7b	92.1	89.7	69.0	89.5	62.8	62.0	62.6	62.8	62.6
vanilla	instructblip-vicuna-7b	67.9	20.1	18.7	48.0	33.7	35.8	33.7	31.2	36.5
+D <sup>AUG</sup>	instructblip-vicuna-7b	55.5	41.4	38.4	56.5	27.3	28.2	27.6	27.2	30.7
Ours	instructblip-vicuna-7b	95.6	89.8	93.7	88.1	57.6	56.4	58.8	59.6	57.0

### C.8. Evaluation on Reasoning-Enhanced (“Thinking”) Models

Reasoning-enhanced “thinking” models may potentially mitigate modality interference by explicitly reasoning over multimodal inputs. To partially examine this hypothesis, we first evaluate chain-of-thought (CoT) prompting in the main paper (Table 1). While CoT prompting reliably improves reasoning accuracy on clean inputs, it does not reduce modality interference under modality-mismatched perturbations, and the same failure modes persist.

To further study this question, we additionally evaluate **R1-OneVision-7B** (Yang et al., 2025), a multimodal large language model explicitly designed with enhanced reasoning capabilities with a backbone Qwen2.5-VL-7B model. We compare its performance against a strong non-reasoning baseline, **Qwen2.5-VL-7B**, under representative image-heavy and text-heavy OOD settings.

Table 14 reports the results. Despite its stronger reasoning ability, R1-OneVision-7B still exhibits substantial performance degradation under misleading textual perturbations and visual distractors. In contrast, Qwen2.5-VL-7B shows comparable or stronger robustness under the same conditions.

These results suggest that improved reasoning alone is insufficient to resolve modality interference. Without explicit mechanisms to control modality reliance, such as modality-aware perturbation and regularization, even reasoning-enhanced models remain vulnerable to task-irrelevant signals.

We investigated the generated reasoning traces: In some cases the model shows better awareness of irrelevant modalities, but in many cases the model still treats unrelated modality as meaningful evidence and produces long hallucinated interpretations that directly influence the final answer. This confirms that our methods remain necessary for interference mitigation.

## Diagnosing and Mitigating Modality Interference in Multimodal Large Language Models

Table 13. Ablation study without modality-aware masking. The *No Mask* variant applies adversarial perturbations to all modalities across all datasets. Results are reported on image-heavy (Caltech-101) and text-heavy (OpenBookQA) benchmarks, together with overall VQA accuracy.

Model	Caltech-101				OpenBookQA		VQA Overall
	Orig	Mislead Text	OCR Text	RandPixels	Real Image	Screenshot	
LLaVA-1.5-7B (Vanilla)	97.0	57.4	92.8	62.4	56.4	50.2	63.8
LLaVA-1.5-7B (Ours, No Mask)	98.1	96.3	93.5	79.5	78.1	62.7	61.5
LLaVA-1.5-7B (Ours)	<b>99.3</b>	<b>98.9</b>	<b>99.0</b>	<b>81.8</b>	<b>81.0</b>	<b>81.8</b>	<b>66.8</b>

Table 14. Evaluation of reasoning-enhanced “thinking” models under modality-mismatched perturbations. Results are reported on image-heavy (Caltech-101) and text-heavy (OpenBookQA) tasks.

Model	Caltech-101 (Orig)	Caltech-101 (Mislead Text)	OpenBookQA (RandPixels)	OpenBookQA (Real Image)
R1-OneVision-7B	96.5	84.7	81.2	77.6
Qwen2.5-VL-7B	<b>99.1</b>	<b>97.2</b>	<b>85.9</b>	<b>77.5</b>

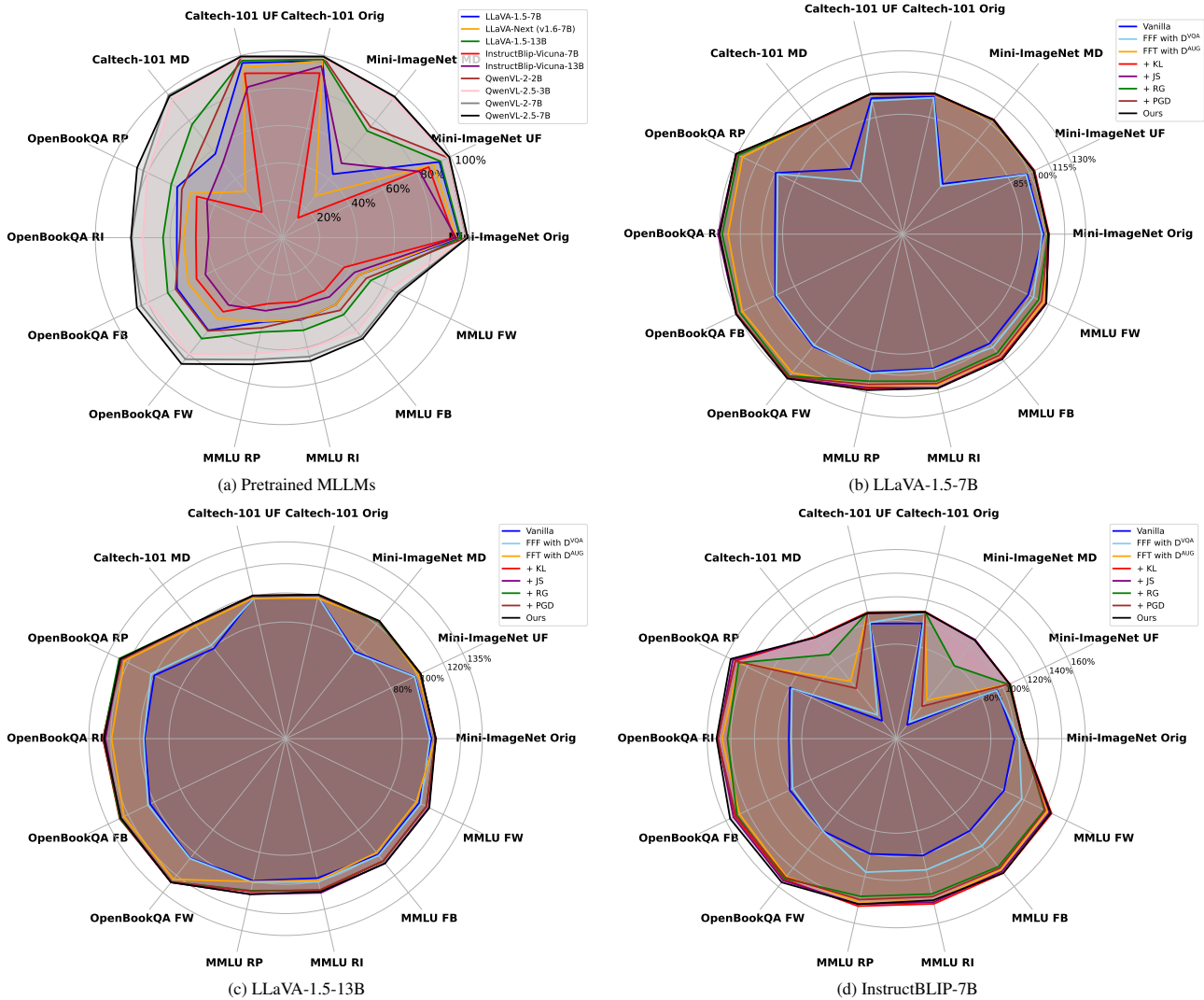


Figure 5. Task-wise robustness under perturbation. Each radar chart shows model accuracy (%) across Mini-ImageNet, Caltech-101 (image-heavy) and OpenBookQA, MMLU (text-heavy) under various perturbations. (a) uses raw accuracy of different pretrained MLLMs directly. (b–d) are normalized relative accuracy of each MLLMs. (We normalize each absolute accuracy into relative accuracy, which refers to absolute tested accuracy / accuracy of vanilla MLLMs in origin setting without perturbation.)

## D. Hyper-Parameter Setting and Training details

Please see Table 15 for more details.

### D.1. Parameter Analysis with adversarial training iterations

To investigate the effect of adversarial strength on model performance, we vary the number of adversarial training iterations from 1 to 5 and evaluate the resulting VQA accuracy. As shown in Figure 6, both LLaVA-1.5-7B and LLaVA-1.5-13B models benefit from adversarial consistency training, with performance peaking at 2-step adversarial training (66.82% and 68.37%, respectively). Notably, excessive iterations (e.g., 4 or 5 steps) may lead to slight degradation, especially in larger models, likely due to over-perturbation and optimization difficulty.

These findings suggest that a moderate adversarial training setting (2 steps with  $\epsilon=1e-3$  and  $\alpha=0.1$  in LLaVA-1.5-7b,  $\epsilon=1e-4$  and  $\alpha=0.1$  in LLaVA-1.5-13b) offers an optimal balance between robustness and training stability, and that model size influences sensitivity to adversarial signal strength.

Table 15. Hyperparameter Settings Example

Category	Setting
<i>Model and Training Strategy</i>	
Base Model	LLaVA-1.5-7B
Finetune Type	Full
Adversarial Type	PGD-alike
Step size $\alpha$	0.1
Epsilon-hall $\epsilon$	0.001
Adversarial Training Steps $T$	2
Consistency Regularization Type	JS
Loss Weight $\lambda_{\text{consistency}}$	0.01
Temperature $\tau$	1
<i>Optimization</i>	
Epochs	1
Batch Size per GPU $ \mathcal{B} $	8
Img/Text Ratio	0.25/0.25
Learning rate	$2 \times 10^{-5}$

Table 16. Dataset Statistics

Dataset	Train	Test
Mini-ImageNet	4935	2000
Caltech-101	8124	1020
OpenBookQA	4957	1000
MMLU	7M	5469
LLaVA-Instruct	624610	-
TextCaps	109765	-
MMBench-EN	-	4377
ScienceQA-IMG	-	4114
SeedBench-IMG	-	14243

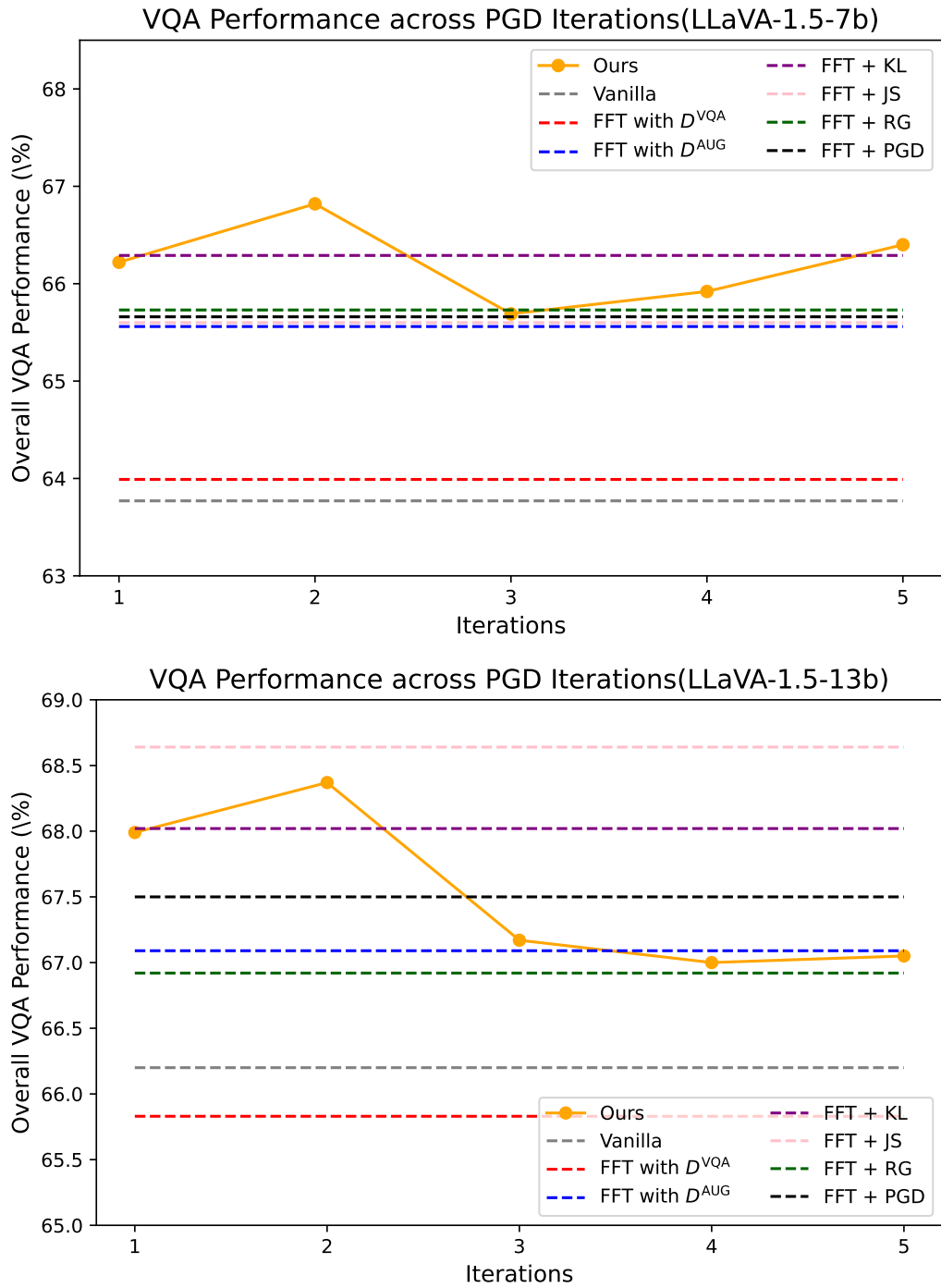


Figure 6. Comparison of VQA performance across adversarial training iterations for different model sizes.

### E. Experiments compute resources

All experiments were conducted on 8×A100 GPUs using DeepSpeed ZeRO-3 (Contributors, 2024) with CPU offloading.

To quantify the computational overhead introduced by our adversarial training, we provide both theoretical FLOPs analysis and empirical wall-clock training time across model scales.

In the standard supervised fine-tuning (SFT) setting, the FLOPs per batch can be approximated as:

$$\text{FLOPs}_{\text{SFT}} \approx B_s \cdot (f_{\text{LLM}} + b_{\text{LLM}}), \tag{10}$$

where  $B_s$  is the batch size,  $f_{\text{LLM}}$  denotes the FLOPs of a forward pass through the LLM, and  $b_{\text{LLM}}$  the backward pass. In our adversarial training, each sample undergoes  $N$  adversarial training steps, each requiring an additional forward pass through the *frozen* LLM. Since gradients are computed only with respect to input embeddings via `torch.autograd.grad`, the overhead is minimal and thus ignored. After perturbation, clean and adversarial inputs are concatenated, resulting in a forward cost of  $2B_s \cdot f_{\text{LLM}}$ , followed by one backward pass. The total cost becomes:

$$\text{FLOPs}_{\text{ADV+SFT}} = B_s \cdot (Nf_{\text{LLM}} + 2f_{\text{LLM}} + b_{\text{LLM}}). \tag{11}$$

The relative overhead compared to vanilla SFT is:

$$\frac{Nf + 2f + b}{f + b}. \tag{12}$$

Assuming  $b_{\text{LLM}} \approx 2f_{\text{LLM}}$ , this simplifies to:

$$\frac{N + 4}{3}. \tag{13}$$

For our default  $N = 1$ , the theoretical FLOPs increase to approximately 1.66× that of SFT.

We further report the actual training time across model scales, as shown in Table 17.

Table 17. Training time (in hours) across model scales.  $\Delta$  denotes additional overhead per adversarial training iteration step.

Model	SFT	SFT + KL	SFT + ADV	Ours (ADV + KL)
Qwen2.5-VL-3B	1.5h	1.5–1.75h	3–3.5h ( $\Delta = 0.5h$ )	3.5–4h ( $\Delta = 0.5h$ )
LLaVA-1.5-7B	4h	4–4.5h	6–6.5h ( $\Delta = 0.5h$ )	6–6.5h ( $\Delta = 0.5h$ )
LLaVA-1.5-13B	10h	10–11h	13–14h ( $\Delta = 1h$ )	13–14h ( $\Delta = 1h$ )

Although the theoretical FLOPs suggest a ~66% increase in cost when  $N = 1$ , the actual wall-clock time increase is much smaller. This is because our designed adversarial training leverages forward-only passes over frozen LLMs,

avoiding costly backward and optimizer updates. As a result, the added runtime remains modest even on large models (e.g., only +2.5h for LLaVA-13B). Moreover, KL consistency training introduces negligible overhead compared to SFT.

### F. Limitations

Our analysis of modality interference is conducted from a coarse-grained perspective, primarily categorizing tasks into image-heavy and text-heavy types. A more fine-grained investigation—such as dynamic attention tracking—could provide deeper insights into how MLLMs rely on or ignore specific modalities during reasoning.

Moreover, while our perturbation strategies (e.g., unrelated facts, misleading descriptions, irrelevant images) effectively reveal failure modes of current MLLMs, they remain heuristic and task-specific. Designing perturbations is, by nature, an open-ended process—one can always propose new forms of misleading inputs. Thus, an ultimate goal is to develop perturbation-agnostic methods that improve robustness without requiring exhaustive enumeration of possible attacks.

While our use of adversarial training represents a strong and generalizable perturbation strategy, it still operates within a defined input space (e.g., embedding-level noise bounded by  $L_\infty$  norms). Hence, adversarial perturbation should be viewed as a practical but partial solution rather than a comprehensive defense. Developing mechanisms that generalize across both semantic and modality perturbations remains an open and challenging direction.

### G. The Use of Large Language Models

We used large language models only to edit the manuscript for clarity, grammar, and academic style. No part of the research design, data analysis, or scientific content relied on language models, and the authors retain full responsibility for the paper’s ideas and conclusions.